

ARTICLE

# PRDM16 suppresses HIF-targeted gene expression in kidney cancer

Anirban Kundu<sup>1</sup>, Hyeyoung Nam<sup>1</sup>, Sandeep Shelar<sup>1</sup>, Darshan S. Chandrashekar<sup>2</sup>, Garrett Brinkley<sup>1</sup>, Suman Karki<sup>1</sup>, Tanecia Mitchell<sup>1</sup>, Carolina B. Livi<sup>3</sup>, Phillip Buckhaults<sup>4</sup>, Richard Kirkman<sup>1</sup>, Yawen Tang<sup>5</sup>, Glenn C. Rowe<sup>5</sup>, Shi Wei<sup>2,6</sup>, Sooryanarayana Varambally<sup>2,6</sup>, and Sunil Sudarshan<sup>1,6,7</sup>

**Analysis of transcriptomic data demonstrates extensive epigenetic gene silencing of the transcription factor PRDM16 in renal cancer. We show that restoration of PRDM16 in RCC cells suppresses in vivo tumor growth. RNaseq analysis reveals that PRDM16 imparts a predominantly repressive effect on the RCC transcriptome including suppression of the gene encoding semaphorin 5B (SEMA5B). SEMA5B is a HIF target gene highly expressed in RCC that promotes in vivo tumor growth. Functional studies demonstrate that PRDM16's repressive properties, mediated by physical interaction with the transcriptional corepressors C-terminal binding proteins (CtBP1/2), are required for suppression of both SEMA5B expression and in vivo tumor growth. Finally, we show that reconstitution of RCC cells with a PRDM16 mutant unable to bind CtBPs nullifies PRDM16's effects on both SEMA5B repression and tumor growth suppression. Collectively, our data uncover a novel epigenetic basis by which HIF target gene expression is amplified in kidney cancer and a new mechanism by which PRDM16 exerts its tumor suppressive effects.**

## Introduction

Renal cell carcinoma (RCC) is one of the top 10 most common malignancies affecting both men and women (Siegel et al., 2018). The most frequent histology is clear cell RCC (ccRCC). The most common tumor-initiating event in this malignancy is alteration of the von Hippel-Lindau (VHL) gene, which encodes an E3 ubiquitin ligase. The VHL complex targets proteins for proteosomal degradation. The most well-characterized substrates of VHL are the hypoxia inducible factors (HIF-1 $\alpha$  and HIF-2 $\alpha$ ; Ivan et al., 2001; Maxwell et al., 1999). VHL loss, silencing, or mutation can result in the aberrant stabilization of HIFs. Many HIF- $\alpha$  target genes encode proteins that can promote renal carcinogenesis. These include factors critical to fundamental processes such as angiogenesis (vascular endothelial growth factor), cell proliferation and/or survival (TGF- $\alpha$ ), and extracellular matrix modulation (matrix metalloproteinase 1).

While VHL loss is critical for HIF signaling, recent evidence indicates that additional mechanisms operate in RCC to promote the HIF axis. Moreover, as there are many HIF target genes, identification of those critical to RCC progression remains poorly characterized. The molecular events that fine-tune this signaling axis may provide novel insight into tumor growth and

progression. Recent studies indicate a role for epigenetics in the modulation of HIF signaling in RCC. Improved understanding of the epigenetic mechanisms that modulate the HIF axis and the target genes amplified by these additional mechanisms may lead to novel insights with biomarker and/or therapeutic implications. Here, we identify epigenetic silencing of the transcription factor PR (PRD1-BF1-RIZ1 homologous) domain-containing 16 (PRDM16) in RCC. Loss of PRDM16 leads to the enhanced expression of the HIF-responsive gene semaphorin 5B (SEMA5B), which supports RCC growth in vivo. Collectively, our studies support a novel mechanism by which renal cancer cells modulate HIF-dependent signaling to promote tumor growth.

## Results

### PRDM16 is epigenetically silenced in RCC

We recently reported an integrative genomic analysis of DNA methylation and gene expression landscapes of kidney cancer that included three sample groups: normal kidney ( $n = 9$ ), primary RCC ( $n = 9$ ), and metastatic RCC tissue deposits ( $n = 26$ ; Nam et al., 2019). We analyzed the transcriptomes of the

<sup>1</sup>Department of Urology, University of Alabama at Birmingham, Birmingham, AL; <sup>2</sup>Department of Pathology, University of Alabama at Birmingham, Birmingham, AL; <sup>3</sup>Department of Molecular Medicine, University of Texas Health Sciences Center at San Antonio, San Antonio, TX; <sup>4</sup>South Carolina College of Pharmacy, University of South Carolina, Columbia, SC; <sup>5</sup>Department of Medicine, University of Alabama at Birmingham, Birmingham, AL; <sup>6</sup>O'Neal Comprehensive Cancer Center, Birmingham AL; <sup>7</sup>Birmingham Veterans Affairs Medical Center, Birmingham, AL.

Correspondence to Sunil Sudarshan: [sudarshan@uab.edu](mailto:sudarshan@uab.edu).

© 2020 Kundu et al. This article is distributed under the terms of an Attribution-Noncommercial-Share Alike-No Mirror Sites license for the first six months after the publication date (see <http://www.rupress.org/terms/>). After six months it is available under a Creative Commons License (Attribution-Noncommercial-Share Alike 4.0 International license, as described at <https://creativecommons.org/licenses/by-nc-sa/4.0/>).

deposited data (series GSE105261) using GEO2R (National Center for Biotechnology Information [NCBI]) and identified the top 250 most differentially expressed genes (regardless of directionality) based on the F-statistic, an analysis that combines t-statistics for all pairwise comparisons when more than two sample groups are present (Table S1). Genes previously described to have altered expression in RCC were also altered in this dataset, including *SFRP1* (decreased expression in tumors compared with normal) and *NDUFA4L2* (increased expression in tumors compared with normal; Gumz et al., 2007; Minton et al., 2016). Based on rank ordering of the F-statistic, we noted that *PRDM16* was among the genes with the most significant differential expression in this dataset. We observed reduced expression with tumor progression (Fig. S1 A). *PRDM16* encodes for the transcription factor PRDM16. PRDM16 has a prominent role in brown fat physiology (Kajimura et al., 2008; Seale et al., 2007, 2008). Consistent with prior studies in mouse tissues, we identified expression of *PRDM16* in brown adipose tissue (with relatively low expression in white adipose tissue (Fig. 1 A). Among the tissues with the highest expression of this factor are the kidney, heart, and small intestine. Consistent with these data, transcriptomic analysis of human tissues also demonstrates relatively high expression of *PRDM16* in the kidney (Fig. S1 B; Uhlen et al., 2017). Using real-time quantitative PCR, we confirmed the loss of *PRDM16* mRNA expression in tumor samples of a series of patient-matched tumor/normal pairs (Fig. 1 B). Moreover, we observed reduced *PRDM16* mRNA in a panel of RCC lines relative to RPTEC (renal proximal tubule epithelial cells) untransformed renal epithelial cells (Fig. S1 C). Consistent with the mRNA data, immunoblotting of patient-matched samples also demonstrated reduced PRDM16 protein expression in tumor (Fig. 1 C). Furthermore, immunohistochemical staining of normal kidney demonstrated nuclear PRDM16 expression in renal proximal tubular epithelium, the cellular origin of ccRCC (Fig. 1 D and Fig. S1 D). In contrast, PRDM16 expression was not detected in tumor cells of ccRCC. PRDM16 is a member of the PR domain-containing family. We therefore examined the relative expression of PRDM16 as well as other PR domain-containing family members in The Cancer Genome Atlas (TCGA) data using the UALCAN analysis portal (<http://ualcan.path.uab.edu>; Chandrashekar et al., 2017). Consistent with our observations, analysis of TCGA RNA sequencing (RNaseq) data demonstrates a significant loss of expression of *PRDM16* in ccRCC (Fig. 1 E). We also analyzed proteomics data on clear cell renal cancer from the National Cancer Institute (NCI)-sponsored Clinical Proteomic Tumor Analysis Consortium, which was recently reported using the UALCAN analysis portal (Chen et al., 2019; Clark et al., 2019). These data clearly demonstrate reduced PRDM16 protein in RCC and therefore validate both our immunoblot and immunohistochemistry analyses (Fig. 1 F). In comparison to the prominent down-regulation of PRDM16, only modest (~1.3-fold) reductions in PRDM2 and PRDM4 expression were found in RCC (Fig. S1 E). Notably, among tumor samples, lower *PRDM16* expression is associated with worsened prognosis (Fig. 1 G). However, no significant association with outcome was observed for PRDM2 or PRDM4 (data not shown).

The robust down-regulation of PRDM16 in RCC tissues and cell lines led us to consider possible mechanisms by which it is silenced. The most common tumor-initiating event in ccRCC is alteration of the *VHL* gene (Gnarra et al., 1994). Loss of VHL function results in the aberrant stabilization of the HIFs. Analysis of TCGA data demonstrates that *PRDM16* is silenced in both *VHL* mutant and WT ccRCC relative to normal kidney (Fig. 1 H). Prior studies indicate that PRDM family members may be a subject to epigenetic regulation in cancer (Tan et al., 2014; Watanabe et al., 2007). We therefore evaluated whether DNA methylation could promote *PRDM16* silencing. We first analyzed methylome (450K array) and gene expression data on tumor samples from the TCGA dataset. Based on analysis using the University of California, Santa Cruz (UCSC) genome browser, there are three CpG-rich regions around the *PRDM16* transcription start site (depicted in Fig. 1 I). We identified the 10 CpG loci within this region whose methylation has the strongest anticorrelation with *PRDM16* mRNA expression. Half of these sites (include the top four most anticorrelated loci) reside within CpG island no. 1 upstream of *PRDM16* (shown in yellow; Fig. 1 I and Fig. S2 A). A plot demonstrating the inverse relationship between CpG site methylation and PRDM16 mRNA expression for the CpG locus (cg01514538) with the strongest negative correlation is shown in Fig. 1 J. TCGA methylome data were generated with standard bisulfite sequencing, which cannot resolve between 5-methylcytosine (5mC) and 5-hydroxymethylcytosine (5hmC). While 5mC accumulation in gene promoters is associated with silencing, 5hmC accumulation has been shown to accumulate at enhancer regions and may be associated with increased expression (Tsagaratou et al., 2014). We therefore assessed DNA 5mC levels at CpG sites within this island via chromatin immunoprecipitation-quantitative PCR (ChIP-qPCR) using an antibody specific to 5mC. We found significant enrichment of 5mC within the region encompassing cg01514538 in RCC cell lines RXF-393 and RCC4 (Fig. 1 K). Moreover, 5mC levels were higher in multiple regions encompassing CpG sites within this island (cg05346286, cg03969902, and cg01514538) in tumor relative to normal kidney in multiple patient-matched samples (Fig. 1 L). As a positive control, we identified increased 5mC enrichment in RCC (as compared with matched normal kidney) of the promoter of *ESSRG*, a gene that we recently reported to be methylated in RCC (Fig. S2, B and C; Nam et al., 2019). Collectively, these data demonstrate that the *PRDM16* promoter region is methylated in RCC. Analysis of TCGA data demonstrates reduced *PRDM16* expression in other tumors such as lung adenocarcinoma with promoter methylation (Fig. S2, D-F).

#### PRDM16 reduces RCC cell growth in vitro and in mice xenograft models

The prominent methylation and silencing of *PRDM16* in RCC led us to consider the biological significance of this finding. As noted previously, PRDM16 has a prominent role in brown fat metabolism and has previously been shown to induce expression of the mitochondrial metabolism-related transcription factors in adipocytes including PGC-1 $\alpha$  and ERR- $\gamma$  (encoded by *PPARGC1A* and

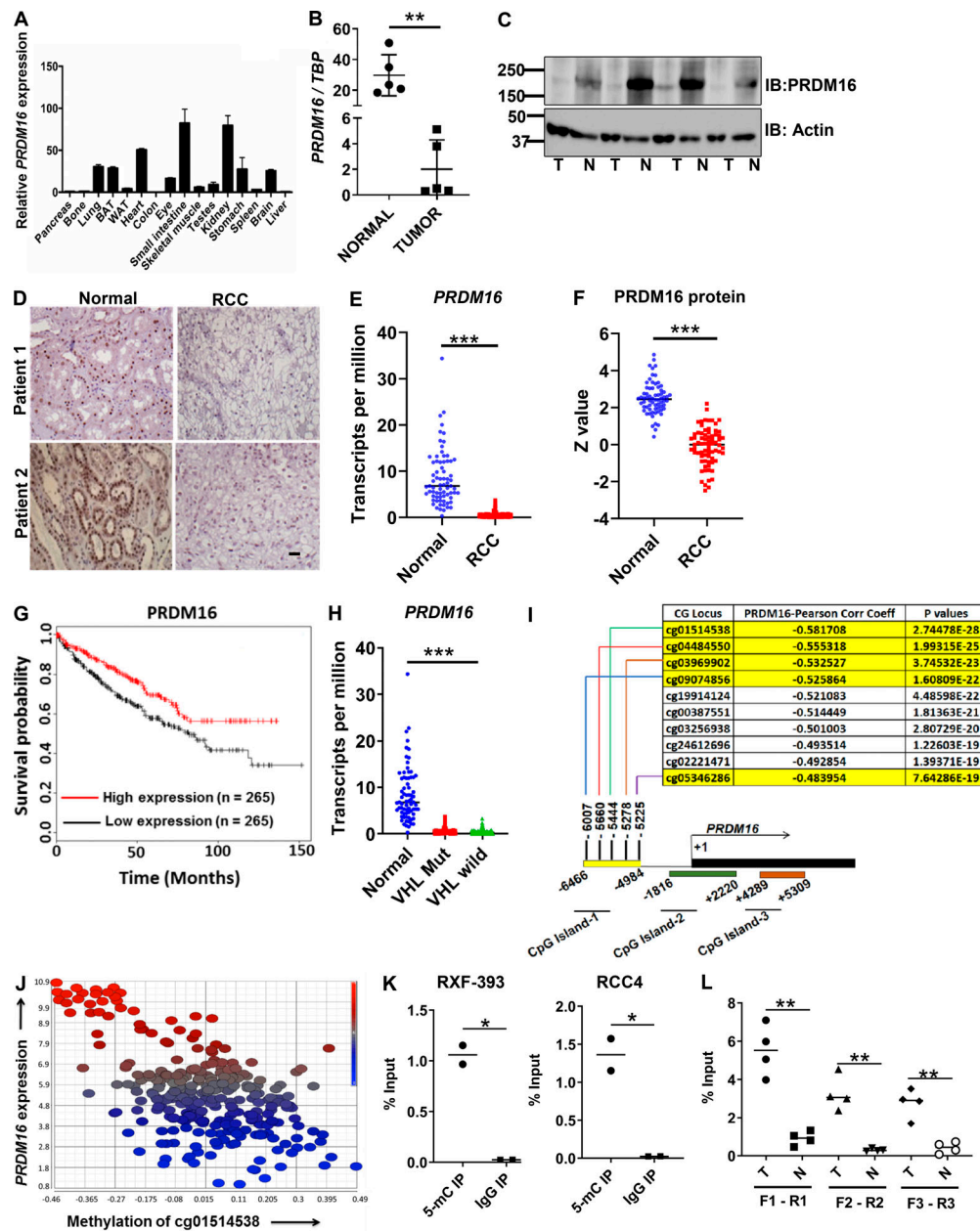


**Figure 1. PRDM16 expression is lost in RCC by promoter hypermethylation.** (A) Relative *PRDM16* mRNA expression was assayed in murine tissues via qPCR ( $n = 3$ ; BAT, brown adipose tissue; WAT, white adipose tissue). (B) Relative *PRDM16* mRNA expression in patient-matched tumor/normal pair samples ( $n = 5$ ) normalized to TBP. Error bars in A and B indicate mean  $\pm$  SD. (C) Immunoblot (IB) analysis of PRDM16 protein expression in patient-matched tumor (T)/normal (N) pair samples ( $n = 4$ ). (D) PRDM16 immunohistochemistry in RCC tumor and corresponding normal tissue ( $\times 400$  magnification; scale bar in black, 20  $\mu$ m). (E) Analysis of PRDM16 mRNA expression in normal kidney and ccRCC using TCGA clear cell kidney cancer (KIRC) dataset. Horizontal bars represent median. Student's  $t$  test,  $***, P < 0.0001$ . (F) Analysis of PRDM16 protein levels in ccRCC and normal kidney using TCGA Clinical Proteomic Tumor Analysis Consortium (CPTAC). Data analyzed with the UALCAN analysis portal. Horizontal bars represents median. Student's  $t$  test,  $***, P < 0.0001$ . (G) Kaplan–Meier survival curve analysis of patients from the TCGA dataset on ccRCC based on expression of PRDM16 mRNA ( $P = 0.0032$ ). (H) PRDM16 expression in normal kidney ( $n = 72$ ), *VHL* mutant RCC ( $n = 217$ ), and *VHL* WT RCC ( $n = 205$ ). Data extracted from TCGA KIRC dataset. One-way ANOVA,  $***, P < 0.0001$ . (I) TCGA data on RCC was analyzed to identify the top CpG loci with the strongest negative correlation between methylation and PRDM16 expression. Loci in yellow are located within a putative CpG island upstream of the *PRDM16* transcription start site (+1). Locations of CpG island loci (yellow, green, and red bars) are depicted in base pairs relative to transcription start site designated as +1. (J) Plot of relative PRDM16 mRNA expression (y axis) as a function of methylation ( $\beta$ ) level (x axis) at the top-ranked CpG locus cg01514538.  $\beta$  levels are all mean-centered. (K) ChIP was performed on RCC4 ( $n = 2$ ) and RXF-393 ( $n = 2$ ) RCC cells with anti-5mC and control IgG antibodies. Enrichment was calculated with the percent input method using primers (F3/R3) within a putative CpG island upstream of the *PRDM16* transcription start site. (L) DNA from patient-matched tumor/normal pairs ( $n = 4$  pairs) were assessed for 5mC levels via ChIP qPCR using three different primer pairs (F1/R1, F2/R2, and F3/R3) within the upstream CpG island. Result (K) is representative of two independent experiments. For K and L, horizontal bars represent median; Student's  $t$  test,  $*$ ,  $P < 0.05$ ,  $**$ ,  $P < 0.005$ . Mut, mutant.

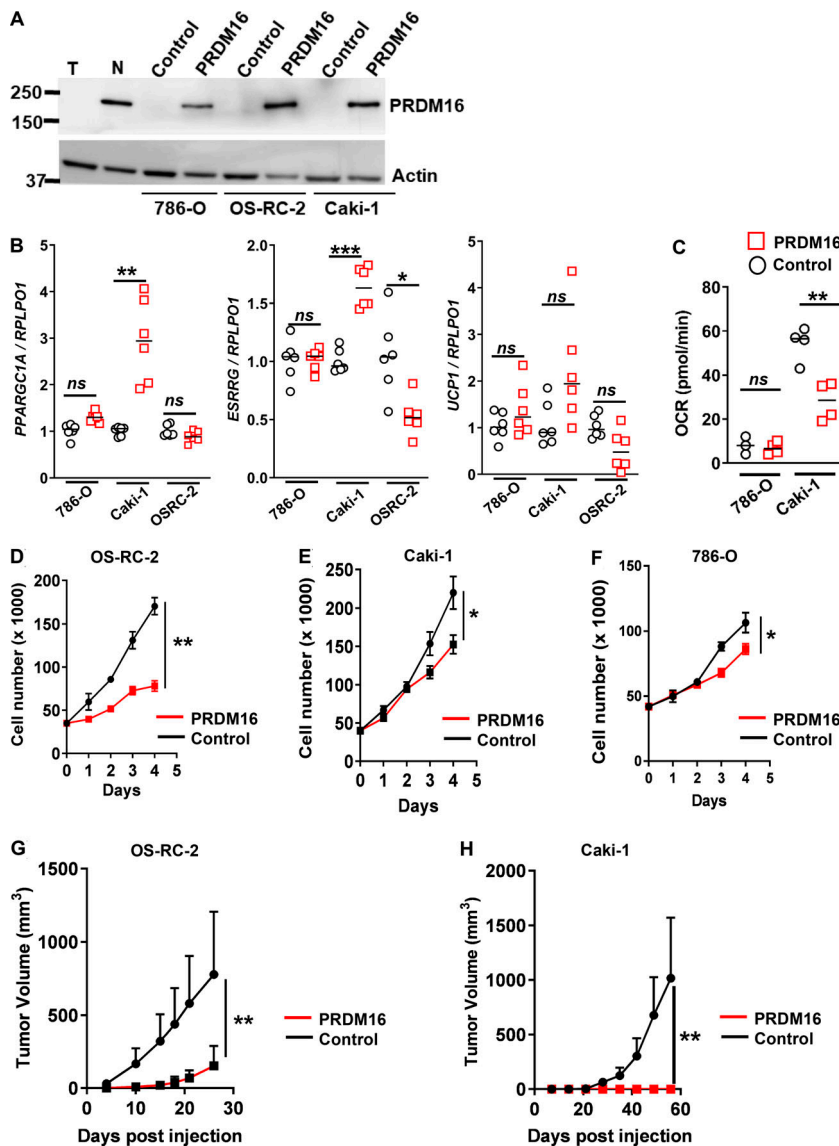


**Figure 2. Effect of PRDM16 on mitochondrial metabolism and tumor phenotypes in RCC cells. (A)** PRDM16 immunoblot of samples from normal kidney, RCC primary tissue, and RCC cell lines (786-O, OS-RC-2, Caki-1) stably transduced with control vector or PRDM16. T, tumor; N, normal. **(B)** qPCR analysis of *PPARGCIA*, *ESRRG*, and *UCP1* expression in RCC cells (786-O, Caki-1, OS-RC-2) containing either control vector or PRDM16. **(C)** Oxygen consumption rate analysis of RCC cells (786-O, Caki-1) stably transduced with control vector or PRDM16. **(D–F)** Proliferation of PRDM16 transduced RCC cells (OS-RC-2, Caki-1, 786-O) relative to control vector ( $n = 3$  per experimental group). For B and C, horizontal bars represent median. **(G and H)** In vivo xenograft experiment comparing tumor growth in RCC cells (OS-RC-2,  $n = 7$  per group; Caki-1,  $n = 6$  per group) plus or minus PRDM16 reconstitution. A–C are representative of two independent experiments. D–F are representative of minimum three independent experiments. For D–H, data are mean  $\pm$  SD. Student's *t* test, \*,  $P < 0.05$ , \*\*,  $P < 0.005$ , and \*\*\*,  $P < 0.0001$ ; ns, not significant.

*ESRRG*) as well as uncoupling protein 1 (*UCP1*; Kajimura et al., 2008; Seale et al., 2007, 2008). Notably, the expression of *PPARGCIA* and *ESRRG* has previously been shown to be reduced in RCC (LaGory et al., 2015; Nam et al., 2019). We therefore assessed the effects of PRDM16 on the expression of these factors in RCC cells via stable transduction in RCC cells. Immunoblotting demonstrates that the level of PRDM16 protein expression achieved by transduction is comparable to that in normal kidney (Fig. 2 A). Ectopic expression of PRDM16 in multiple RCC lines examined failed to show a consistent effect on the expression of these factors (Fig. 2 B). In line with these data, we did not observe an increase in oxygen consumption (Fig. 2 C). Prior studies have demonstrated that agents such as forskolin and rosiglitazone can enhance PRDM16 function in mouse brown fat cells (Ohno et al., 2012; Seale et al., 2007). Both agents were able to promote PRDM16's induction of *ESRRG* in multiple lines (Fig. S3, A and B). However, no consistent effects were observed on the expression of *PPARGCIA* or *UCP1* or on oxygen consumption (Fig. S3, A–C). We did observe that PRDM16 restoration could

suppress proliferation in OSRC-2 cells and to a lesser extent in Caki-1 and 786-O RCC cells (Fig. 2, D–F). Moreover, PRDM16 reduced transwell migration, wound healing, and in vitro invasion of RCC cells (Fig. S4, A–C). These data prompted us to assess the effect of PRDM16 on in vivo tumor growth. In both OSRC-2 and Caki-1 cells, restoration of PRDM16 expression significantly suppressed RCC xenograft growth (Fig. 2, G and H).

#### PRDM16 predominantly represses transcription in RCC

Our observation that PRDM16 can suppress in vitro proliferation and in vivo tumor growth despite the lack of induction of *PPARGCIA* and *ESRRG* (under basal conditions in the absence of rosiglitazone and forskolin) led us to consider if there were effects of PRDM16 outside of the established role in cell metabolism. We performed RNaseq analysis in 786-O RCC cells plus or minus exogenous expression of PRDM16. Analysis demonstrated that PRDM16 exerts a repressive effect on the transcriptional landscape (Fig. 3, A and B). Of the genes altered with PRDM16 restoration, two thirds of genes were down-regulated, whereas

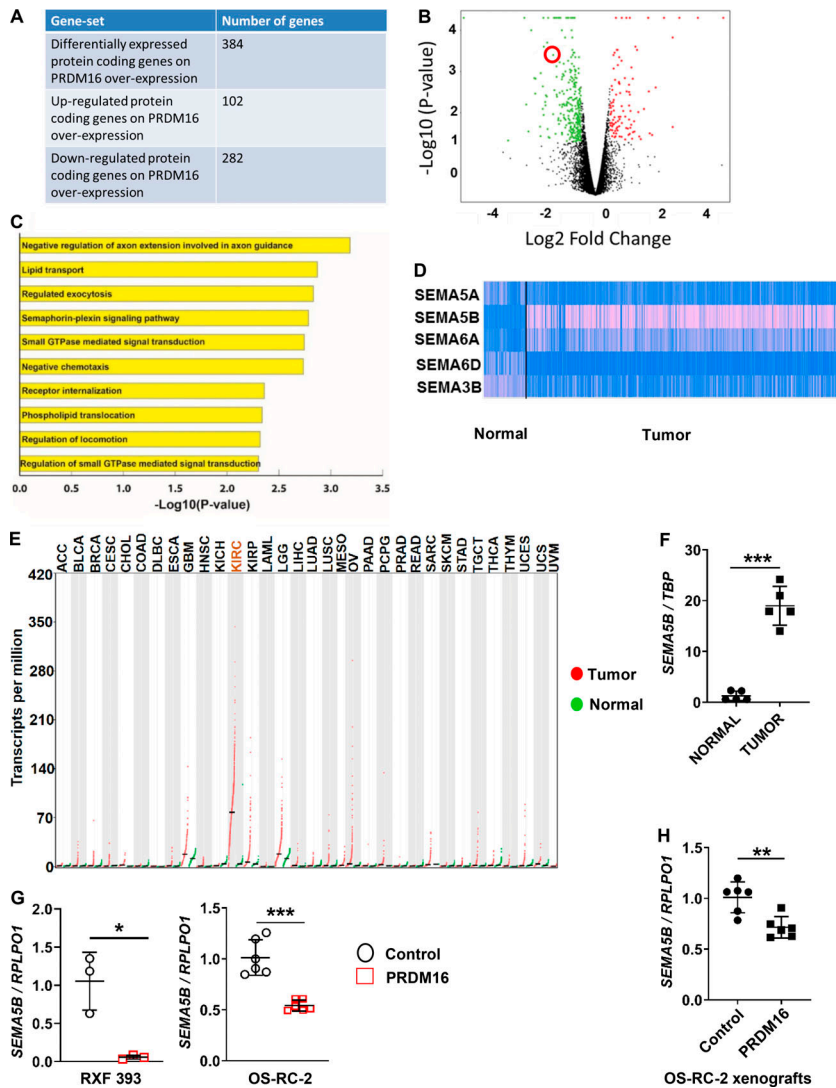


**Figure 3. PRDM16 suppresses SEMA5B expression.** (A) 786-O RCC cells were transduced with control vector (n = 2) or PRDM16 (n = 2) lentivirus followed by RNaseq analysis to identify differentially expressed genes. (B) Volcano plot of differentially expressed genes upon restoration of PRDM16. SEMA5B (red circle) among genes suppressed by PRDM16 in 786-O cells. (C) Gene ontology enrichment analysis of genes with reduced expression upon PRDM16 restoration. (D) Expression of SEMA family members suppressed by PRDM16 in normal kidney and RCC samples from TCGA KIRC dataset. IB, immunoblot. (E) Analysis of SEMA5B expression in all tumor and normal samples from TCGA. SEMA5B expression in ccRCC (referred to as KIRC) is represented in brown text. Data extracted using GEPIA web server. (F) qPCR analysis of SEMA5B mRNA expression in patient-matched tumor/normal pairs (n = 5). (G) RCC cells (RXF-393, n = 3; OS-RC-2, n = 6) were stably transduced with PRDM16 or control vector and assessed for SEMA5B expression via qPCR. Data are mean ± SD and are representative of two independent experiments. (H) OSRC-2 xenografts (plus or minus PRDM16) were assayed for SEMA5B expression via qPCR. Student's t test, \*, P < 0.05, \*\*, P < 0.005, and \*\*\*, P < 0.0001.

only one third of genes were up-regulated. Pathway analysis revealed that PRDM16 suppresses the expression of genes involved in axonal guidance and signaling, including members of the semaphorin (SEMA) family of transmembrane proteins (Fig. 3, B and C; and Table S2). SEMAs are a class of signaling molecules whose function has been primarily studied in the nervous system. SEMAs bind to their receptors, referred to as plexins, which are known to associate with and activate tyrosine kinases (Artigiani et al., 2004; Giordano et al., 2002; Oinuma et al., 2004). Notably, increased SEMA5B in RCC was also identified in our initial GEO2R analysis as a differentially expressed gene (Table S1 and Fig. S5 A). We assessed the relative expression of SEMA family members repressed by PRDM16 in the TCGA dataset on ccRCC and found that SEMA5B had the highest expression in ccRCC (Fig. 3 D). Furthermore, analysis of TCGA data across all tumor types demonstrates that SEMA5B expression is highest in ccRCC among all other tissues, benign or malignant (Fig. 3 E). RT-qPCR analysis of matched tumor/normal pairs from ccRCC patients confirmed increased SEMA5B (Fig. 3 F). We validated the suppression of SEMA5B by PRDM16 in OSRC-2 and RXF-393 RCC cells (Fig. 3 G). Additionally, this

finding was validated in vivo as SEMA5B mRNA expression was lower in PRDM16 expressing xenograft tumors relative to control tumors (Fig. 3 H).

**SEMA5B is a HIF target gene**

The high expression of SEMA5B in ccRCC led us to consider if VHL has any role on the regulation of SEMA5B expression. We first characterized SEMA5B mRNA expression via RT-qPCR analysis and observed that SEMA5B expression was low in VHL WT lines. VHL mutant lines had variable expression (Fig. 4 A). We therefore examined the expression of SEMA5B as a function of VHL expression in paired RCC lines (786-O and RCC4) plus or minus VHL. Parental RCC4 cells express both HIF-1α and HIF-2α whereas parental 786-O cells express only HIF-2α. As VHL is known to promote the degradation of HIF, reconstitution of VHL led to an expected reduction in the expression of the HIF target gene GLUT1 in both RCC4 and 786-O cells (Fig. 4 B). VHL restoration in RCC4 cells resulted in reduced expression of PDK1, a known HIF-1α target gene (Fig. 4 B; Kim et al., 2006; Papandreou et al., 2006). Consistent with the absence of HIF-1α expression in 786-O cells, restoration of VHL in these cells had no

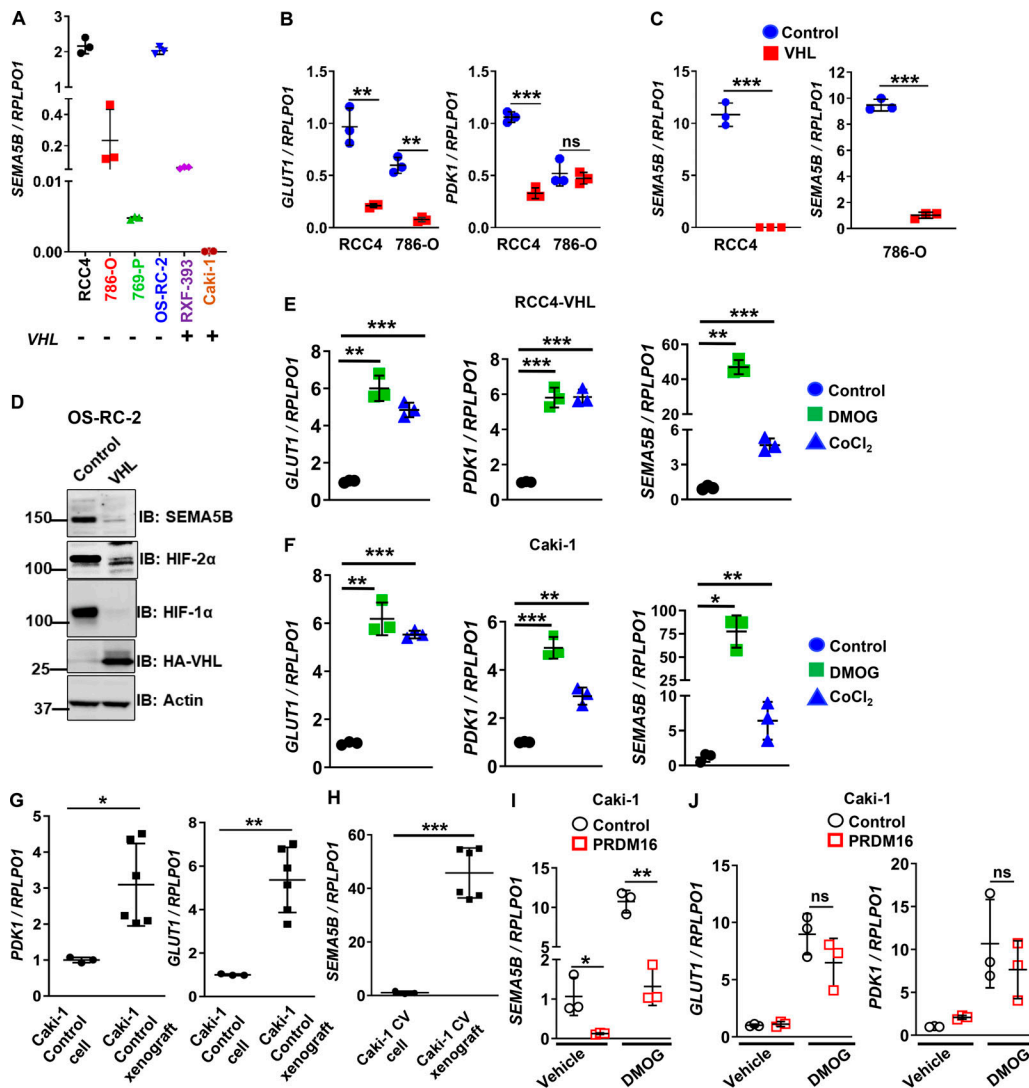


**Figure 4. HIF-induced expression of SEMA5B is antagonized by PRDM16.** (A) Relative *SEMA5B* expression in a panel of VHL WT and mutant RCC cells ( $n = 3$  each) by qPCR. (B and C) *VHL* mutant RCC4 and 786-O cells were stable transduced with control vector or WT *VHL* construct and assessed for transcript levels of canonical HIF target genes (*GLUT1*, *PDK1*) along with *SEMA5B* via qPCR ( $n = 3$  each). (D) *SEMA5B*, HIF-1, and HIF-2 protein expression in OS-RC-2 cells plus or minus *VHL* (HA-tagged). (E and F) RCC4/*VHL* and Caki-1 (*VHL* WT) cells were treated with the hypoxia-mimetic agents DMOG and  $\text{CoCl}_2$ . Cells were analyzed by qPCR for the expression of HIF target genes *GLUT1* and *PDK1* as well as *SEMA5B* ( $n = 3$  each). (G and H) Caki-1 cells transduced with control vector were grown under both in vitro ( $n = 3$ ) and in vivo conditions ( $n = 6$ ). RNA was extracted and assayed for *GLUT1*, *PDK1*, and *SEMA5B* mRNA levels via qPCR. (I and J) Caki-1 cells ( $n = 3$ ) transduced with control vector or PRDM16 lentivirus were cultured plus or minus DMOG and assayed for mRNA expression of *SEMA5B*, *GLUT1*, and *PDK1*. A–F, I, and J are representative of at least two independent experiments. Data are mean  $\pm$  SD. Student's *t* test, \*,  $P < 0.05$ , \*\*,  $P < 0.005$ , and \*\*\*,  $P < 0.0001$ ; ns, not significant.

effect on *PDK1*. Restoration of *VHL* led to a dramatic reduction in *SEMA5B* mRNA (Fig. 4 C). Consistent with *VHL*'s role in HIF regulation, restoration of *VHL* in OSRC-2 cells led to reduced HIF-1 $\alpha$  and HIF-2 $\alpha$  protein (Fig. 4 D). In concert with our transcript data, *VHL* restoration also led to reduced *SEMA5B* protein (Figs. 4 D and S5, D and E). As further evidence for a role of HIF in the regulation of *SEMA5B*, we examined the effects of hypoxia mimetics dimethylxalylglycine (DMOG) and  $\text{CoCl}_2$  in *VHL*-expressing RCC cells (RCC4/*VHL* and Caki-1). Both DMOG and  $\text{CoCl}_2$  promoted induction of the known HIF target genes (*GLUT1* and *PDK1*) along with *SEMA5B* (Fig. 4, E and F). The marked induction of *SEMA5B* expression under hypoxia mimetics led us to consider if the relatively hypoxic environment in vivo could also

induce *SEMA5B*. We therefore examined expression of canonical HIF target genes (Fig. 4 G) and *SEMA5B* (Fig. 4 H) in Caki-1 cells (transduced with a control vector) grown in vivo compared with cells grown under standard in vitro culture conditions. Caki-1 cells are *VHL* WT and therefore do not demonstrate increased HIF protein expression under normoxic conditions. While we observed a modest but significant increase in *PDK1* and *GLUT1* expression in vivo (Fig. 4 G), we found a marked increased (>40-fold) of *SEMA5B* expression in vivo relative to in vitro (Fig. 4 H). We next determined if PRDM16 could suppress the HIF-mediated induction of *SEMA5B*. Consistent with parental cells, DMOG treatment of Caki-1 cells stably transduced with control vector led to a significant increase in *SEMA5B*

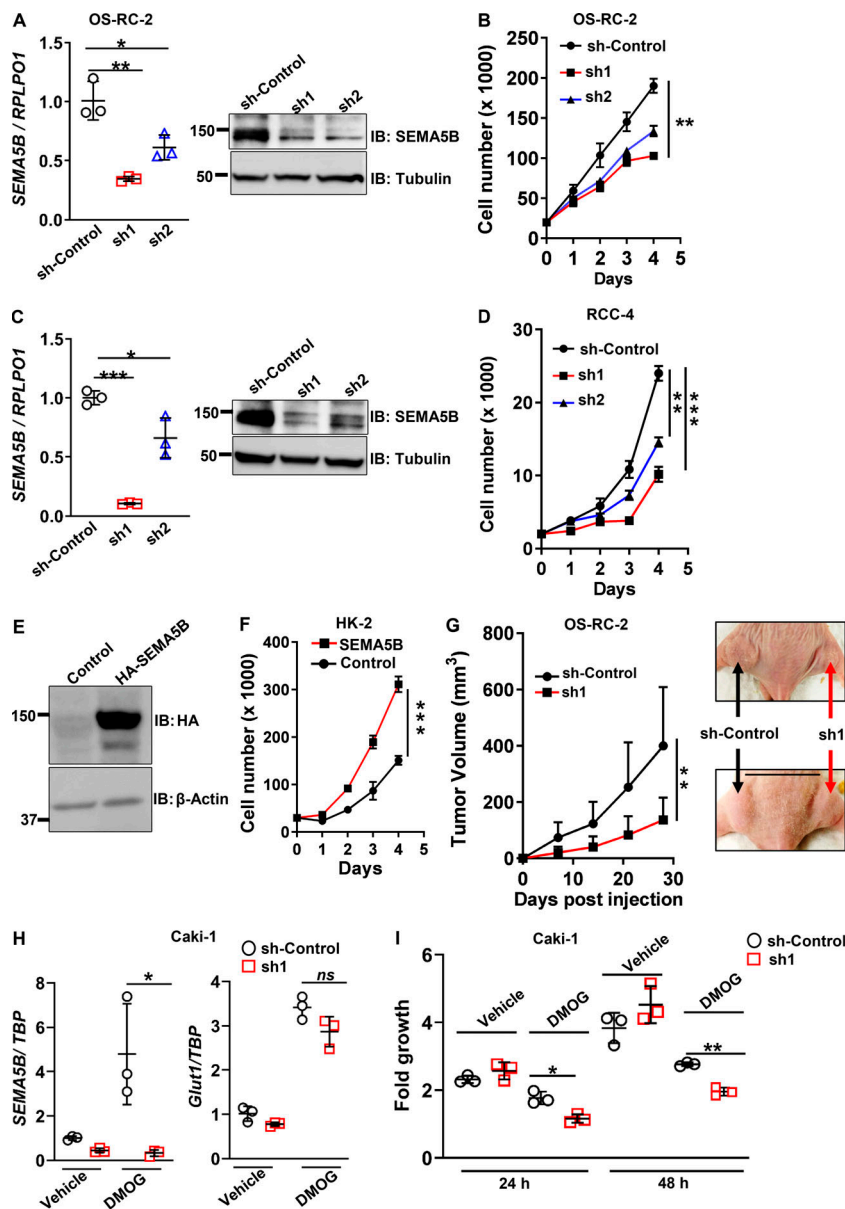


**Figure 5. SEMA5B promotes RCC proliferation and in vivo tumor growth.** (A–D) OS-RC-2 ( $n = 3$ ) and RCC4 cells ( $n = 3$ ) were stably transduced with control shRNA or shRNAs targeting *SEMA5B* (sh1 and sh2). Polyclonal pools were assayed for *SEMA5B* mRNA and protein expression (A and C) and in vitro cell proliferation (B and D). IB, immunoblot. (E and F) Stably transduced HK-2 ( $n = 3$ ) cells with control vector or HA-*SEMA5B* construct were assayed for HA-*SEMA5B* expression and for cell proliferation. (G) Control and *SEMA5B* knock-down OS-RC-2 cells were injected into the flanks of athymic nude mice ( $n = 8$ /group) and assayed for tumor growth over time (scale bar in black, 4 cm). (H and I) Caki-1 cells ( $n = 3$ ) were stably transduced with control shRNA or sh1 targeting *SEMA5B*. Cells were assayed for *SEMA5B* and *GLUT1* expression (H) and in vitro cell growth in the presence of 300 mM DMOG (I). Data in A, C, E, and H are representative of two independent experiments. Data in B, D, F, and I are representative of at least three independent experiments. Data are mean  $\pm$  SD. Student's *t* test, \*,  $P < 0.05$ , \*\*,  $P < 0.005$ , and \*\*\*,  $P < 0.0001$ ; ns, not significant.

expression. However, the expression of PRDM16 blunted the ability of DMOG to induce *SEMA5B* (Fig. 4 I) but not other HIF target genes (Fig. 4 J).

**SEMA5B promotes RCC growth in vitro and in vivo**

We next assessed the biological significance of elevated *SEMA5B* expression in RCC cells. Prior studies examining the functional significance of increased *SEMA5B* in RCC were limited in scope (Hirota et al., 2006). We therefore knocked down *SEMA5B* expression via stable introduction of shRNA with two different nonoverlapping constructs in the OS-RC-2 cell line. We confirmed target gene knockdown via qPCR and immunoblotting (Fig. 5 A). Both knockdown clones demonstrated reduced proliferation relative to control vector cells (Fig. 5 B). Similar results were obtained in RCC4 cells (Fig. 5, C and D). We next performed a gain-of-function analysis by expressing *SEMA5B* (hemagglutinin [HA]-tagged) in nontransformed HK2 renal epithelial cells.

*SEMA5B* expression was confirmed by immunoblotting (Fig. 5 E). Increased *SEMA5B* expression promoted proliferation in HK2 cells (Fig. 5 F). Similar results were obtained when *SEMA5B* was expressed in 769-P cells (Fig. S5, B and C). Based on these data, we examined the role of *SEMA5B* in vivo. Notably, we found that *SEMA5B* knockdown significantly reduced OSRC-2 xenograft growth (Fig. 5 G). We also examine *SEMA5B*'s functional significance in the setting of intact VHL but with HIF activation. VHL WT Caki-1 cells were cultured in the presence of the hypoxia mimetic DMOG, which results in increased *SEMA5B* and *GLUT1* expression (see sh-Control in Fig. 5 H). As expected, *SEMA5B* shRNA reduced *SEMA5B* expression without effects on *GLUT1* expression (see sh-1 in Fig. 5 H). Knockdown of *SEMA5B* in cells cultured with DMOG resulted in reduced proliferation (Fig. 5 I). In contrast, *SEMA5B* knockdown has no effect on proliferation in vehicle-treated cells that have low *SEMA5B* expression.

### PRDM16–C-terminal binding protein (CtBP) interaction is responsible for the suppression of *SEMA5B* and of RCC cell growth

Given the functional significance of *SEMA5B* in promoting RCC proliferation and in vivo tumor growth, we next investigated the mechanism by which PRDM16 repressed *SEMA5B* expression. Prior studies have demonstrated that PRDM16's effect on transcription, either promoting or suppressing, are mediated in part by interacting proteins (Kajimura et al., 2008; Seale et al., 2007). As noted before, PRDM16 is expressed at high levels in the kidney, but its function has not been characterized. To gain insight into PRDM16 biology in the kidney, we assessed for PRDM16-interacting proteins in HEK293T cells. We selected these cells because they are renal in origin. To facilitate our studies, we ectopically expressed an N-terminal FLAG-tagged version of PRDM16 in these cells followed by immunoprecipitation (IP) of cell lysates with anti-FLAG antibody and IgG antibody control. Immunoprecipitated fractions were electrophoresed in an SDS-PAGE gel followed by in-gel trypsin digestion of the lanes with subsequent analysis by liquid chromatography–mass spectrometry (LC-MS). Notably, CtBP-1/2 were among the most enriched proteins (Table S3). Prior studies indicate that PRDM16 interaction with CtBPs, which function as corepressors, is critical to the suppression of the white fat gene expression program in brown adipose tissue (Kajimura et al., 2008). We confirmed this interaction by immunoprecipitation in HEK293T and OS-RC-2 cells (Fig. 6, A and B; compare lanes 1 and 2 of immunoprecipitates). Prior studies have identified that PRDM16 interaction with CtBP1 and CtBP2 is dependent on the PLDLS motif in PRDM16 (amino acids 804–808) motif (Kajimura et al., 2008). Mutation of this motif to PLASS disrupts PRDM16/CtBP interaction in adipocytes. In agreement with these data, mutation of this motif in PRDM16 disrupts CtBP interaction (Fig. 6, A and B; compare lanes 1 and 3 of immunoprecipitates) in HEK293T and OS-RC-2 cells. Immunoblotting of inputs from both cell lines demonstrated no significant effects on CtBP protein expression. We next examined the ability of WT and mutant PRDM16 to suppress *SEMA5B* mRNA and protein expression (Fig. 6, C and D). Consistent with prior data, WT PRDM16 significantly reduced *SEMA5B* expression, whereas mutant PRDM16 had no effect on *SEMA5B*. Analysis of ChIP sequencing (ChIP-seq) tracks deposited by the Encyclopedia of DNA Elements (ENCODE) consortium using the UCSC genome browser demonstrates the presence of a CtBP binding site within 2 kb of the *SEMA5B* transcription start site (Fig. 6 E). We therefore assessed if PRDM16 or CtBP can bind to this region via ChIP-qPCR. Both WT and mutant PRDM16 demonstrated similar binding to this region relative to IgG control. In contrast, CtBP binding to this region was significantly reduced in RCC cells expressing mutant PRDM16 as compared with WT PRDM16 (Fig. 6 F). Collectively, these data indicate that CtBPs' interaction with PRDM16 promotes CtBPs' binding to the *SEMA5B* promoter.

Based on these data, we next assessed whether PRDM16's interaction with CtBPs is critical for their effects on tumor phenotypes. Whereas WT PRDM16 transduced RCC cells demonstrated reduced proliferation compared with control

cells, RCC cells transduced with mutant PRDM16 failed to demonstrate any decrease in proliferation (Fig. 6 G). Furthermore, PRDM16 mutant transduced cells readily grew in vivo in contrast with WT PRDM16-expressing cells, which demonstrated markedly reduced tumor growth (Fig. 6 H). We next assessed the functional significance of PRDM16's repression of *SEMA5B* expression. We therefore reintroduced both PRDM16 and *SEMA5B* in addition to control vector and PRDM16 alone (please see Western blot, Fig. 6 I). OSRC-2 RCC cells with PRDM16 restored demonstrate reduced *SEMA5B* as well as reduced proliferation and colony formation (Fig. 6, J and K). However, restoration of *SEMA5B* can partially rescue PRDM16's effects on proliferation and colony formation (Fig. 6, J and K). These data indicate that PRDM16's effects are, at least in part, *SEMA5B* dependent. Collectively, these data demonstrate that PRDM16 antagonizes the proliferative effects of the HIF/*SEMA5B* axis in RCC. Furthermore, these data indicate that PRDM16's effects on both the HIF/*SEMA5B* axis and on tumor growth are dependent on its interaction with CtBPs.

### Discussion

Here, we report that *PRDM16* is silenced in the most common type of RCC and that this factor can suppress xenograft tumor growth. We demonstrate a novel role for PRDM16 in the suppression of the HIF-responsive gene *SEMA5B*. Moreover, our data suggest a role for *SEMA5B* in tumor growth. Additionally, these are the first data to reveal that PRDM16's transcriptional repressive properties can promote tumor-suppressive effects. Specifically, PRDM16's interaction with the corepressor proteins CtBP1/2 is critical for its suppression of *SEMA5B* expression, proliferation, and in vivo tumor growth. As outlined in Fig. 7, our data have relevance to both *VHL* WT tumors, which are hypoxic, and *VHL* mutant tumors, which are pseudohypoxic. In either case, HIF stabilization ensues with promotion of target gene expression.

These are the first data, to our knowledge, to demonstrate a role for PRDM16 in the suppression of solid tumor growth. Prior studies have implicated loss of PRDM family members including PRDM16 in lung cancer (Tan et al., 2014). However, the functional significance of this loss was not fully elucidated as in vivo studies are lacking. Moreover, we would like to point out that prior studies examined *PRDM16* methylation through methodologies that use standard bisulfite sequencing. However, bisulfite sequencing cannot resolve between 5mC and 5hmC. This is notable as recent studies indicate that 5hmC enrichment may be associated with activation, as opposed to suppression, of gene expression. Hence, resolution of these marks is critical to determine the precise role of DNA methylation in gene expression.

The majority of data linking PRDM16 with malignancy is in the context of leukemia. In leukemia, gene arrangements of *PRDM16* result in loss of the PR domain, which is associated with methyltransferase activity (Lahortiga et al., 2004). Zhou et al. (2016) recently demonstrated that this domain is critical for suppressing leukemia development in a murine mixed lineage

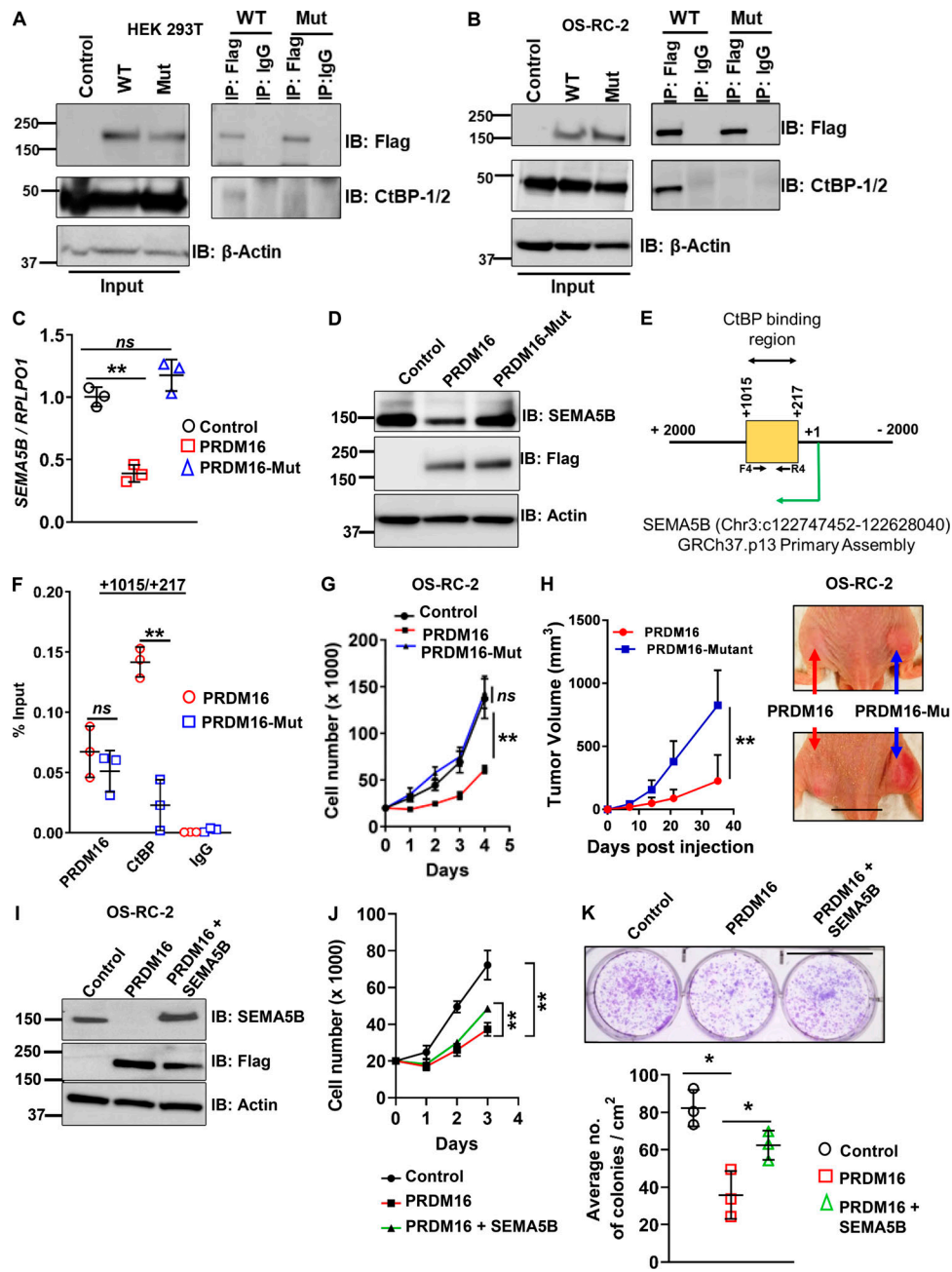


**Figure 6. PRDM16 interaction with CtBPs is required for suppression of both SEMA5B expression and tumor phenotypes.** (A and B) HEK293T cells were transiently transfected and OS-RC-2 cells were stably transduced with control vector, FLAG-tagged WT PRDM16, or mutant (Mut) PRDM16 construct. Immunoprecipitation (IP) with FLAG followed by immunoblotting (IB) for CtBP1/2 was performed to assess the presence of PRDM16/CtBP interaction. IgG pulldown is included as a control. (C and D) Control vector, WT PRDM16, and mutant PRDM16 OS-RC-2 cells (polyclonal pool,  $n = 3$ ) were assayed for SEMA5B expression via qPCR and immunoblot. (E) Schematic representation of a CtBP binding site within  $\pm 2,000$  kb of the SEMA5B transcription start site in the UCSC genome browser. (F) WT and mutant PRDM16 transduced OS-RC-2 cells were assessed for binding of PRDM16 and CtBP to the SEMA5B promoter via ChIP-qPCR with anti-FLAG (PRDM16) or anti-CtBP antibodies. Control IgG antibody is included. Enrichment was calculated with the percent input method using the primer pair F4-R4 as shown in E. (G) Control vector, WT PRDM16, and mutant PRDM16 transduced OS-RC-2 cells were assayed for in vitro proliferation ( $n = 3$ ). (H) Stably transduced PRDM16 or mutant PRDM16 OS-RC-2 cells were injected into the flanks of athymic nude mice ( $n = 8$ /group) and assayed for tumor growth over time (scale bar in black, 3.5 cm). (I-K) OS-RC-2 cells stably transduced with either control vector, PRDM16 alone, or PRDM16 and SEMA5B together. Cells were assayed for protein expression, proliferation ( $n = 3$ /group), and colony formation ( $n = 3$ /group; scale bar in black, 3.5 cm). Data in A-D, G, and I-K are representative of two independent experiments. Data are mean  $\pm$  SD. Student's  $t$  test, \*,  $P < 0.05$ , \*\*,  $P < 0.005$ ; ns, not significant.

leukemia model. In particular, PRDM16's H3K4 methyltransferase activity promoted expression of the of the transcription factor GFI1b, which in turn suppressed the expression of *Hox* genes. Of note, they observed progressively increased

PRDM16 gene methylation with malignant transformation in this model. These data suggest that PRDM16 methylation, and therefore its silencing, in cancer is not simply a random occurrence. Mechanistic insight of this silencing warrants further study.

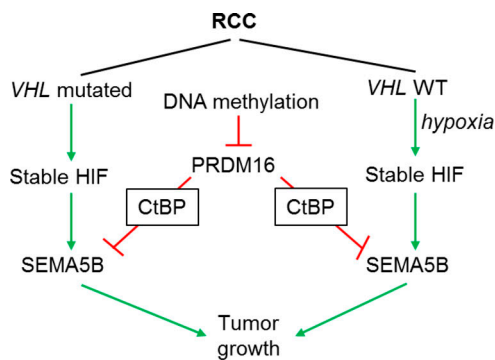


Figure 7. Model for PRDM16 mediated SEMA5B silencing in RCC.

Our data indicate that the mechanism of PRDM16's role in tumor biology is context dependent and that PRDM16's transcriptional repressive properties are responsible for its suppression of tumor phenotypes in the context of kidney cancer. PRDM16's repressive effects have been well-characterized in the context of adipocyte biology, where it has been shown to selectively repress white fat gene expression. Our data indicate that *SEMA5B* is one of the targets of the PRDM16/CtBP repressive complex in renal cancer. SEMAs have recently been found to affect tumor progression by various mechanisms, including modulation of tumor angiogenesis (Basile et al., 2007; Zhou et al., 2017). In addition, SEMA-plexin interaction can induce phosphorylation of tyrosine kinases including Met and Ron to promote invasiveness and tumor metastasis (Conrotto et al., 2005; Giordano et al., 2002). SEMA family members can be broadly divided into eight groups. Class 5 SEMAs, consisting of SEMA5A and SEMA5B, are expressed in vertebrates. There may be some functional redundancy between SEMA5A and 5B. Both can bind plexins A1 and A3, suggesting the possibility of compensation if one or the other is inhibited (Matsuoka et al., 2011). However, the low expression of SEMA5A in RCC (Fig. 3 D) would argue against a compensatory effect upon SEMA5B knockdown. The high expression of SEMA5B in ccRCC coupled with our loss-of-function studies in RCC cells suggest opportunities for intervention. Recent studies indicate that SEMA interaction with their plexin receptor is targetable (Matsunaga et al., 2016). Alternatively, the intracellular signaling cascades activated by SEMA5B might also be targetable. Although ccRCC is refractory to traditional chemotherapeutic agents as well as radiation, the efficacy of small molecule inhibitors has led to the approval of several tyrosine kinase inhibitors for advanced RCC. Hence, delineation of the events of the downstream signaling events of SEMA5B-plexin interaction warrants further investigation.

Our data add to the increasing complexity of HIF signaling in ccRCC. Mutations of *VHL* are highly prevalent in ccRCC. Our data add to the growing body of evidence of the role of epigenetics in the amplification of HIF signaling in RCC. *PBRM1* is commonly mutated in ccRCC (Varela et al., 2011). This is a component of the SWI/SNF (SWItch/Sucrose Non-Fermentable) chromatin remodeling complex. Recent studies indicate that alteration of *PBRM1* promotes the expression of HIF-responsive

genes (Gao et al., 2017). Recent studies have also implicated DNA hypomethylation in promoting HIF signaling. We recently demonstrated evidence of promoter hypomethylation in RCC tissues of several HIF target genes, including those encoding enzymes such as HK2 and aldolase C which are involved in glycolysis (Nam et al., 2019). Experimental studies of RCC by Vanharanta et al. (2013) demonstrate that DNA demethylation promotes the expression of the HIF target gene *CYTIP* in an in vivo model of ccRCC lung colonization. Our studies support a novel mechanism for the promotion of HIF signaling through DNA hypermethylation of the *PRDM16* gene, which results in enhanced expression of the HIF target *SEMA5B* gene.

As there are a multitude of HIF target genes, a challenge in the field has been deciphering which of these targets are critical to RCC progression. HIFs as well as their target genes may have contrasting properties, i.e., tumor-promoting or -suppressing. In RCC, HIF-1 $\alpha$  is thought to be tumor suppressive whereas HIF-2 $\alpha$  is thought to be tumor-promoting (Kondo et al., 2003; Shen et al., 2011). While on balance HIF-1 $\alpha$  is tumor suppressive, there is a subset of HIF-1 $\alpha$  responsive genes that has experimentally been shown to promote phenotypes such as proliferation including *NDUFA4L2* (Minton et al., 2016). Our findings herein, as well as previously published data, indicate that epigenetic alterations can amplify HIF signaling in RCC. Hence, identification of HIF-1 $\alpha$  and/or HIF-2 $\alpha$  targets, amplified through various epigenetic mechanisms, could pinpoint those genes most contributory to renal carcinogenesis and tumor progression.

There are limitations of our study. While we demonstrate a role for PRDM16 in suppressing *SEMA5B*, there are likely other targets responsible for PRDM16's effect on RCC cells. These may include other SEMA family members based on the results of our transcriptomic studies. In addition, we may need to consider the transcriptional activating properties of PRDM16. Prior studies in adipocytes demonstrate that PRDM16 induces the expression of *PPARGCA* and *ESRRG* genes. Work by our group and others demonstrates reduced expression of these factors in ccRCC (LaGory et al., 2015; Nam et al., 2019). Additionally, both factors have a known role in the transcription of nuclear encoded genes involved in mitochondrial metabolism, e.g., TCA cycle enzymes and nuclear encoded respiratory chain subunits. Although we saw only modest effects on these factors in vitro that were variable between RCC lines, we cannot exclude effects in vivo.

In summary, our data demonstrate a role for *PRDM16* silencing in ccRCC. Our studies suggest that this factor is involved in modulating HIF-mediated *SEMA5B* expression. These data provide novel insight into the contribution of epigenetics in regulating HIF signaling in ccRCC. Moreover, they provide new lines of study with the potential for therapeutic interventions in tumors driven by the HIF-SEMA5B axis.

## Materials and methods

### Cell culture

786-O-*VHL* or control (empty) vector was obtained from W.G. Kaelin Jr. (Dana-Farber Cancer Institute, Boston, MA) and were cultured in DMEM. RCC4 (kindly provided by P. Ratcliffe, University of Oxford, Oxford, UK) and HK2 cells were also cultured

in DMEM. The Caki-1 cell line was cultured in MEM, and RPMI 1640 media was used for OS-RC-2 and RXF393 cells. HEK-293T cells were grown in DMEM containing 4.5 g/liter glucose. Media for these cell lines were supplemented with 10% fetal bovine serum and 1× penicillin streptomycin. 786-O, Caki-1, 769-P, and HK2 cells were acquired from the American Type Culture Collection. RXF-393 cells were acquired from the NCI. RPTEC cells were obtained from Lonza, and cells were cultured in renal epithelial cell growth basal media. Cell lines were periodically screened for *Mycoplasma*.

#### Plasmids and antibodies

Human *PRDM16* cDNA was purchased from Genecopoeia. Human *SEMA5B* cDNA was acquired from TRANSOMIC technologies. HA-VHL plasmid was acquired from W.G. Kaelin Jr. via Addgene. shRNA constructs (from Sigma-Aldrich) are as follows: pLKO.1-shControl (SHC002), pLKO.1-shSEMA5B1 (TRCN0000060474), and pLKO.1-shSEMA5B2 (TRCN0000060473). Sources of antibodies used in this study are as follows: PRDM16 from Thermo Fisher Scientific (720206); CtBP-1/2 from Active Motif (61261); Flag (for immunoblotting and immunoprecipitation; F1804) *SEMA5B* (HPA066548) from Sigma-Aldrich; Flag (for ChIP; 14793), HA (3724), and HIF-1 $\alpha$  (14179) from Cell Signaling Technology; HIF-2 $\alpha$  (GTX632015) from GeneTex; normal IgG (12-371) from Millipore; and  $\beta$ -actin (ab49900) from Abcam.

#### Gene expression profiling

Gene expression array data from RCC tissues and normal kidney were generated following our previously described protocol with the Illumina Human HT-12 V4.0 expression beadchip (Nam et al., 2019). The raw data and processed data have been uploaded in the Gene Expression Omnibus under accession no. GSE105261. The RNaseq of WT and PRDM16-overexpressing 786-O cells was done in replicates. Adapter sequences and low-quality reads were trimmed from fastq files using trim\_galore ([https://www.bioinformatics.babraham.ac.uk/projects/trim\\_galore/](https://www.bioinformatics.babraham.ac.uk/projects/trim_galore/)). With TopHat v2.1.0 (Kim et al., 2013), trimmed raw read sequences were mapped to *Homo sapiens* reference genome (hg38). The aligned reads were assembled into genes, and their abundance was estimated as fragments per kilobase of exon per million fragments mapped using Cufflinks v2.2.1 (Trapnell et al., 2012). Differential expression analysis was performed using the Cuffdiff module of Cufflinks. Genes with absolute fold change of greater than or equal to  $\geq 1.5$  and P value  $< 0.05$  were considered as differentially expressed genes. The raw and processed data have been uploaded to the Gene Expression Omnibus under accession no. GSE130049. The Database for Annotation, Visualization and Integrated Discovery v6.7 (Huang et al., 2009) was used for gene ontology enrichment analysis on differentially expressed genes.

#### Lentivirus transduction

Plasmid DNAs were transfected into HEK293T cells for production of lentiviral particles. 4  $\mu$ g of lentiviral vector plasmid, 2  $\mu$ g of the gag-pol packaging plasmid, and 1  $\mu$ g of pMD.G (VSV-G) plasmid were transfected with FuGENE6 (Promega). Supernatants were harvest 48 h after transfection and filtered with a 0.45  $\mu$ m pore size filter. Viral extract was then used to

transduce target cells. The lentivirus-infected cells were selected with puromycin.

#### Oxygen consumption measurements

To measure oxygen consumption rate (OCR) and extracellular acidification rate, Seahorse XFe96 Analyzer (Agilent Technologies) was used as previously described (Isono et al., 2016). The seeding density of cells was 30,000–50,000 cells per well. The following day, cells were washed with extracellular flux media (pH 7.4) and allowed to equilibrate for 1 h before measuring basal OCR/ECAR.

#### TCGA methylation and gene expression analysis

For bioinformatic analyses of *PRDM16*, TCGA KIRC Kidney Clear Cell Carcinoma HumanMethylation450 methylation values, HiSeqV2 gene expression values, and clinical data were downloaded from the UCSC Cancer Genomics browser. Statistical tests were performed using the Partek genomics suite. To identify cg loci that are hypermethylated in primary tumor tissue versus normal tissue, a *t* test of differences in the tumor vs. normal mean  $\beta$  values was performed for all cg loci, and resulting *t*-statistic and unadjusted P values were calculated. To identify cg loci that were inversely associated with PRDM16 gene expression in primary tumors, the PRDM16 gene expression values were compared with the methylation values of cg loci, and Pearson correlation coefficients (*r*) and unadjusted P values were calculated. TCGA gene expression analysis and survival analysis were performed using the UALCAN web portal (Chandrashekar et al., 2017) and KM-plotter web portal (Nagy et al., 2018), respectively. Pancancer analyses across multiple TCGA datasets were performed with the Gene Expression Profiling Interactive Analysis web server (Tang et al., 2017).

#### In vitro and in vivo assays for tumor phenotypes

Cell proliferation, wound healing, Boyden chamber migration, and matrigel-based invasion assays were performed to investigate in vitro tumor phenotypes as described earlier (Shelar et al., 2018; Shim et al., 2014). For in vivo xenograft tumor studies, immunodeficient nude (Nu/Nu) mice were obtained from Jackson Laboratory or Charles River and fed a standard chow diet. Cells in sterile PBS were mixed with an equal volume of matrigel and injected ( $2 \times 10^6$  cells/injection) subcutaneously in the flanks of 5–6-wk-old nude mice. Caliper measurements of growing tumors were taken periodically, and the tumor volumes were calculated using the formula ( $L \times W^2/2$ ), where “W” is the smallest diameter and “L” is the largest perpendicular diameter.

#### RNA isolation and qPCR analysis

Total RNA from human tissues was isolated with the RNeasy Mini Kit (Qiagen). RNA from culture cells were extracted with Direct-zol RNA miniprep kit (Zymo Research). cDNA was generated using a High-Capacity cDNA Reverse Transcription kit (Applied Biosystems). qPCR analysis was performed using the Taqman Gene Expression Master reagent mixed with Taqman primers and analyzed with the QuantStudio™ 6K Flex Real-Time PCR System (Applied Biosystems). mRNA expression levels were normalized to human TATA-binding protein (TBP) or human large ribosomal protein RPLP01, and the normalized cycle

threshold (Ct) values were quantified using the double delta Ct analysis. qPCR data represent relative expression. In general, controls in experimental data are normalized to a value of 1. Indicated Taqman primers were predesigned from Applied Biosystems as follows: *PRDM16* (Hs00922682\_m1), *SEMA5B* (Hs00400720\_m1), *PPARGCIA* (Hs00173304\_m1), *ESRRG* (Hs00976243\_m1), *UCPI* (Hs01084772\_m1), *GLUT1* (Hs00892681\_m1), *PDK1* (Hs01561847\_m1), *RPLP01* (Hs99999902\_m1), and *TBP* (Hs00427620\_m1).

### Co-immunoprecipitation and immunoblotting

All immunoprecipitation steps were performed at 4°C. Cells expressing Flag-tagged PRDM16 WT or PRDM16 mutant were lysed in buffer X (50 mM Hepes, pH 7.5, 150 mM NaCl, 0.1% NP-40, and 1 mM EDTA) containing 1× protease/phosphatase inhibitor (Thermo Fisher Scientific). After clearing, 50 μl slurry of a protein A/G-agarose (Santa Cruz Biotechnology, Inc.) and 2 μg of anti-Flag or control IgG antibody was added to 2 mg of the extracted proteins and rotated for 16 h. Next, the beads were spun down at 600 g, and the immunoprecipitates were washed thrice with buffer Y (20 mM Tris-HCl, pH 8.0, 150 mM NaCl, and 2 mM EDTA) for 10 min each with rotation. Finally, the beads were boiled in 2× Laemmli buffer to elute the immunoprecipitated proteins. Protein samples prepared in Laemmli buffer were resolved in 4–15% SDS-PAGE (Biorad) followed by transfer onto polyvinylidene difluoride membrane (Immobilon P, Millipore) using standard procedures. The membranes were blocked with either 3% BSA or 5% skim milk and probed with specific antibodies.

### ChIP-qPCR

To validate hypermethylation of CpG islands located in the upstream of PRDM16 transcription start site, genomic DNA were isolated from RCC cells (RXF-393, RCC4) and patient-matched tumor/normal kidney samples. The 5mC ChIP experiment was performed using the manufacturer's protocol (Cell Signaling Technology, 76853). To study PRDM16-CtBP binding site near the *SEMA5B* transcription start site, stably transfected OS-RC-2 cells expressing either Flag-PRDM16 WT or Flag-PRDM16 mutant were cultured in 150 mm tissue culture dishes to 90% confluency (~6 × 10<sup>6</sup> cells per plate). The ChIP experiment was done following the manufacturer's protocol (Millipore, 17-10085). Input DNA and immunoprecipitated DNA were purified (Zymo Research D4003) and analyzed by quantitative PCR using SYBR green fluorescent dye (Applied Biosystems). The protein-bound DNA was calculated as a ratio to input DNA. Primer sequences used in the ChIP assays are as follows: F1/R1 (5'-CACACGGCTGAAGTCATAG-3'/5'-TTTCACAGCTTTCCCTCTT-3'), F2/R2 (5'-CTGTGGGTAACGAAGTTGCT-3'/5'-ACCTTCAGCCGTGTGTTTC-3'), F3/R3 (5'-CGGCCGAATTGGGATCT-3'/5'-GGAAGGTGGCAGAGCGA-3'), and F4/R4 (5'-GGGAAGGGA CCTCGTGTA-3'/5'-TTAACCTAATCCGGCCAGT-3').

### Statistics

Experimental results are displayed as either by median or by the mean ± SD. One way ANOVA or two-tailed nonparametric Student's *t* test was performed using GraphPad Prism v7.03 to determine significant differences between control and experimental groups as mentioned specifically in the figure legends. *P* values of <0.05 were considered statistically significant.

Kundu et al.

*PRDM16* silencing in kidney cancer

### Study approval

All animal studies were conducted in accordance with the National Institutes of Health guidelines for humane treatment of animals and were approved by the Institutional Animal Care and Use Committee. Deidentified human tissue samples were obtained and used in accordance with a protocol approved by the Institutional Review Board at the University of Alabama at Birmingham. Tissues used for transcriptomic analyses were acquired from Cooperative Human Tissue Network, an NCI-supported resource. Per Cooperative Human Tissue Network protocol, patient consent is obtained for the use of samples for research purposes.

### Online supplemental material

Fig. S1 characterizes PRDM16 expression in normal/tumor tissues and RCC lines. Fig. S2 characterizes PRDM16 expression and methylation in TCGA data. Fig. S3 characterizes the effect of PRDM16 on metabolic factors. Fig. S4 characterizes the effect of PRDM16 on in vitro phenotypes in RCC cells. Fig. S5 characterizes *SEMA5B* expression in ccRCC, the *SEMA5B* effect on proliferation in RCC cells, and *SEMA5B* expression by VHL. Table S1 is a gene list of differentially expressed genes upon analysis of transcriptomic data from normal kidney, primary tissue, and metastatic tissues deposits. Table S2 summarizes RNaseq analysis of 786-O cells plus or minus PRDM16. Table S3 summarizes PRDM16 (FLAG-tagged) interacting protein analysis by LC-MS.

### Acknowledgments

The research reported in this article was supported by National Institutes of Health/NCI grant R01CA200653 and Department of Veterans Affairs grant I01BX002930 (S. Sudarshan) and in part by the University of Alabama at Birmingham O'Neal Comprehensive Cancer Center (P30CA013148).

Author contributions: A. Kundu, H. Nam, S. Shelar, G. Brinkley, S. Karki, T. Mitchell, R. Kirkman, Y. Tang, G.C. Rowe, and S. Wei acquired data. A. Kundu, D.S. Chandrashekar, C.B. Livi, T. Mitchell, P. Buckhaults, S. Varambally, and S. Sudarshan analyzed data. A. Kundu and S. Sudarshan contributed to the conception, design, and writing.

Disclosures: Dr. Livi reported employment at Agilent Technologies not related to published work. No other disclosures were reported.

Submitted: 24 June 2019

Revised: 16 December 2019

Accepted: 21 February 2020

### References

- Artigiani, S., P. Conrotto, P. Fazzari, G.F. Gilestro, D. Barberis, S. Giordano, P.M. Comoglio, and L. Tamagnone. 2004. Plexin-B3 is a functional receptor for semaphorin 5A. *EMBO Rep.* 5:710-714. <https://doi.org/10.1038/sj.embor.7400189>
- Basile, J.R., K. Holmbeck, T.H. Bugge, and J.S. Gutkind. 2007. MT1-MMP controls tumor-induced angiogenesis through the release of semaphorin 4D. *J. Biol. Chem.* 282:6899-6905. <https://doi.org/10.1074/jbc.M609570200>

- Chandrashekar, D.S., B. Basher, S.A.H. Balasubramanya, C.J. Creighton, I. Ponce-Rodriguez, B. Chakravarthi, and S. Varambally. 2017. UALCAN: A Portal for Facilitating Tumor Subgroup Gene Expression and Survival Analyses. *Neoplasia*. 19:649–658.
- Chen, F., D.S. Chandrashekar, S. Varambally, and C.J. Creighton. 2019. Pan-cancer molecular subtypes revealed by mass-spectrometry-based proteomic characterization of more than 500 human cancers. *Nat. Commun.* 10:5679. <https://doi.org/10.1038/s41467-019-13528-0>
- Clark, D.J., S.M. Dhanasekaran, F. Petralia, J. Pan, X. Song, Y. Hu, F. da Veiga Leprevost, B. Reva, T.M. Lih, H.Y. Chang, et al. Clinical Proteomic Tumor Analysis Consortium. 2019. Integrated Proteogenomic Characterization of Clear Cell Renal Cell Carcinoma. *Cell*. 179:964–983.e31. <https://doi.org/10.1016/j.cell.2019.10.007>
- Conrotto, P., D. Valdembrì, S. Corso, G. Serini, L. Tamagnone, P.M. Comoglio, F. Bussolino, and S. Giordano. 2005. Sema4D induces angiogenesis through Met recruitment by Plexin B1. *Blood*. 105:4321–4329. <https://doi.org/10.1182/blood-2004-07-2885>
- Gao, W., W. Li, T. Xiao, X.S. Liu, and W.G. Kaelin Jr. 2017. Inactivation of the PBRM1 tumor suppressor gene amplifies the HIF-response in VHL/-clear cell renal carcinoma. *Proc. Natl. Acad. Sci. USA*. 114:1027–1032. <https://doi.org/10.1073/pnas.1619726114>
- Giordano, S., S. Corso, P. Conrotto, S. Artigiani, G. Gilestro, D. Barberis, L. Tamagnone, and P.M. Comoglio. 2002. The semaphorin 4D receptor controls invasive growth by coupling with Met. *Nat. Cell Biol.* 4:720–724. <https://doi.org/10.1038/ncb843>
- Gnarra, J.R.K., K. Tory, Y. Weng, L. Schmidt, M.H. Wei, H. Li, F. Latif, S. Liu, F. Chen, F.M. Duh, et al. 1994. Mutations of the VHL tumour suppressor gene in renal carcinoma. *Nat. Genet.* 7:85–90. <https://doi.org/10.1038/ng0594-85>
- Gumz, M.L., H. Zou, P.A. Kreinest, A.C. Childs, L.S. Belmonte, S.N. LeGrand, K.J. Wu, B.A. Luxon, M. Sinha, A.S. Parker, et al. 2007. Secreted frizzled-related protein 1 loss contributes to tumor phenotype of clear cell renal cell carcinoma. *Clin. Cancer Res.* 13:4740–4749. <https://doi.org/10.1158/1078-0432.CCR-07-0143>
- Hirota, E., L. Yan, T. Tsunoda, S. Ashida, M. Fujime, T. Shuin, T. Miki, Y. Nakamura, and T. Katagiri. 2006. Genome-wide gene expression profiles of clear cell renal cell carcinoma: identification of molecular targets for treatment of renal cell carcinoma. *Int. J. Oncol.* 29:799–827.
- Huang, W., B.T. Sherman, and R.A. Lempicki. 2009. Systematic and integrative analysis of large gene lists using DAVID bioinformatics resources. *Nat. Protoc.* 4:44–57. <https://doi.org/10.1038/nprot.2008.211>
- Isono, T., T. Chano, J. Yonese, and T. Yuasa. 2016. Therapeutic inhibition of mitochondrial function induces cell death in starvation-resistant renal cell carcinomas. *Sci. Rep.* 6:25669. <https://doi.org/10.1038/srep25669>
- Ivan, M., K. Kondo, H. Yang, W. Kim, J. Valiando, M. Ohh, A. Salic, J.M. Asara, W.S. Lane, and W.G. Kaelin Jr. 2001. HIF1alpha targeted for VHL-mediated destruction by proline hydroxylation: implications for O2 sensing. *Science*. 292:464–468. <https://doi.org/10.1126/science.1059817>
- Kajimura, S., P. Seale, T. Tomaru, H. Erdjument-Bromage, M.P. Cooper, J.L. Ruas, S. Chin, P. Tempst, M.A. Lazar, and B.M. Spiegelman. 2008. Regulation of the brown and white fat gene programs through a PRDM16/CtBP transcriptional complex. *Genes Dev.* 22:1397–1409. <https://doi.org/10.1101/gad.1666108>
- Kim, J.W., I. Tchernyshov, G.L. Semenza, and C.V. Dang. 2006. HIF-1-mediated expression of pyruvate dehydrogenase kinase: a metabolic switch required for cellular adaptation to hypoxia. *Cell Metab.* 3:177–185. <https://doi.org/10.1016/j.cmet.2006.02.002>
- Kim, D., G. Pertea, C. Trapnell, H. Pimentel, R. Kelley, and S.L. Salzberg. 2013. TopHat2: accurate alignment of transcriptomes in the presence of insertions, deletions and gene fusions. *Genome Biol.* 14:R36. <https://doi.org/10.1186/gb-2013-14-4-r36>
- Kondo, K., W.Y. Kim, M. Lechpammer, and W.G. Kaelin Jr. 2003. Inhibition of HIF2alpha is sufficient to suppress pVHL-defective tumor growth. *PLoS Biol.* 1:E83. <https://doi.org/10.1371/journal.pbio.0000083>
- LaGory, E.L., C. Wu, C.M. Taniguchi, C.C. Ding, J.T. Chi, R. von Eyben, D.A. Scott, A.D. Richardson, and A.J. Giaccia. 2015. Suppression of PGC-1α Is Critical for Reprogramming Oxidative Metabolism in Renal Cell Carcinoma. *Cell Rep.* 12:116–127. <https://doi.org/10.1016/j.celrep.2015.06.006>
- Lahortiga, I., X. Agirre, E. Belloni, I. Vázquez, M.J. Larrayoz, P. Gasparini, F. Lo Coco, P.G. Pelicci, M.J. Calasanz, and M.D. Odero. 2004. Molecular characterization of a t(1;3)(p36;q21) in a patient with MDS. MEL1 is widely expressed in normal tissues, including bone marrow, and it is not overexpressed in the t(1;3) cells. *Oncogene*. 23:311–316. <https://doi.org/10.1038/sj.onc.1206923>
- Matsunaga, Y., N.K. Bashiruddin, Y. Kitago, J. Takagi, and H. Suga. 2016. Allosteric Inhibition of a Semaphorin 4D Receptor Plexin B1 by a High-Affinity Macrocyclic Peptide. *Cell Chem. Biol.* 23:1341–1350. <https://doi.org/10.1016/j.chembiol.2016.09.015>
- Matsuoka, R.L., O. Chivatakarn, T.C. Badea, I.S. Samuels, H. Cahill, K. Katayama, S.R. Kumar, F. Suto, A. Chédotal, N.S. Peachey, et al. 2011. Class 5 transmembrane semaphorins control selective Mammalian retinal lamination and function. *Neuron*. 71:460–473. <https://doi.org/10.1016/j.neuron.2011.06.009>
- Maxwell, P.H., M.S. Wiesener, G.W. Chang, S.C. Clifford, E.C. Vaux, M.E. Cockman, C.C. Wykoff, C.W. Pugh, E.R. Maher, and P.J. Ratcliffe. 1999. The tumour suppressor protein VHL targets hypoxia-inducible factors for oxygen-dependent proteolysis. *Nature*. 399:271–275. <https://doi.org/10.1038/20459>
- Minton, D.R., L. Fu, N.P. Mongan, M.M. Shevchuk, D.M. Nanus, and L.J. Gudas. 2016. Role of NADH Dehydrogenase (Ubiquinone) 1 Alpha Subcomplex 4-Like 2 in Clear Cell Renal Cell Carcinoma. *Clin. Cancer Res.* 22:2791–2801. <https://doi.org/10.1158/1078-0432.CCR-15-1511>
- Nagy, Á., A. Lánckzy, O. Menyhárt, and B. Gyórfy. 2018. Validation of miRNA prognostic power in hepatocellular carcinoma using expression data of independent datasets. *Sci. Rep.* 8:9227. <https://doi.org/10.1038/s41598-018-27521-y>
- Nam, H.Y., D.S. Chandrashekar, A. Kundu, S. Shelar, E.Y. Kho, G. Sonpavde, G. Naik, P. Ghatalia, C.B. Livi, S. Varambally, and S. Sudarshan. 2019. Integrative Epigenetic and Gene Expression Analysis of Renal Tumor Progression to Metastasis. *Mol. Cancer Res.* 17:84–96. <https://doi.org/10.1158/1541-7786.MCR-17-0636>
- Ohno, H., K. Shinoda, B.M. Spiegelman, and S. Kajimura. 2012. PPARγ agonists induce a white-to-brown fat conversion through stabilization of PRDM16 protein. *Cell Metab.* 15:395–404. <https://doi.org/10.1016/j.cmet.2012.01.019>
- Oinuma, I., Y. Ishikawa, H. Katoh, and M. Negishi. 2004. The Semaphorin 4D receptor Plexin-B1 is a GTPase activating protein for R-Ras. *Science*. 305:862–865. <https://doi.org/10.1126/science.1097545>
- Papandreou, I., R.A. Cairns, L. Fontana, A.L. Lim, and N.C. Denko. 2006. HIF-1 mediates adaptation to hypoxia by actively downregulating mitochondrial oxygen consumption. *Cell Metab.* 3:187–197. <https://doi.org/10.1016/j.cmet.2006.01.012>
- Seale, P., S. Kajimura, W. Yang, S. Chin, L.M. Rohas, M. Uldry, G. Tavernier, D. Langin, and B.M. Spiegelman. 2007. Transcriptional control of brown fat determination by PRDM16. *Cell Metab.* 6:38–54. <https://doi.org/10.1016/j.cmet.2007.06.001>
- Seale, P., B. Bjork, W. Yang, S. Kajimura, S. Chin, S. Kuang, A. Scimè, S. Devarakonda, H.M. Conroe, H. Erdjument-Bromage, et al. 2008. PRDM16 controls a brown fat/skeletal muscle switch. *Nature*. 454:961–967. <https://doi.org/10.1038/nature07182>
- Shelar, S., E.H. Shim, G.J. Brinkley, A. Kundu, F. Carobbio, T. Poston, J. Tan, V. Parekh, D. Benson, D.K. Crossman, et al. 2018. Biochemical and Epigenetic Insights into L-2-Hydroxyglutarate, a Potential Therapeutic Target in Renal Cancer. *Clin. Cancer Res.* 24:6433–6446. <https://doi.org/10.1158/1078-0432.CCR-18-1727>
- Shen, C., R. Beroukhim, S.E. Schumacher, J. Zhou, M. Chang, S. Signoretti, and W.G. Kaelin Jr. 2011. Genetic and functional studies implicate HIF1α as a 14q kidney cancer suppressor gene. *Cancer Discov.* 1:222–235. <https://doi.org/10.1158/2159-8290.CD-11-0098>
- Shim, E.H., C.B. Livi, D. Rakheja, J. Tan, D. Benson, V. Parekh, E.Y. Kho, A.P. Ghosh, R. Kirkman, S. Velu, et al. 2014. L-2-Hydroxyglutarate: an epigenetic modifier and putative oncometabolite in renal cancer. *Cancer Discov.* 4:1290–1298. <https://doi.org/10.1158/2159-8290.CD-13-0696>
- Siegel, R.L., K.D. Miller, and A. Jemal. 2018. Cancer statistics, 2018. *CA Cancer J. Clin.* 68:7–30. <https://doi.org/10.3322/caac.21442>
- Tan, S.X., R.C. Hu, J.J. Liu, Y.L. Tan, and W.E. Liu. 2014. Methylation of PRDM2, PRDM5 and PRDM16 genes in lung cancer cells. *Int. J. Clin. Exp. Pathol.* 7:2305–2311.
- Tang, Z., C. Li, B. Kang, G. Gao, C. Li, and Z. Zhang. 2017. GEPIA: a web server for cancer and normal gene expression profiling and interactive analyses. *Nucleic Acids Res.* 45(W1):W98–W102. <https://doi.org/10.1093/nar/gkx247>
- Trapnell, C., A. Roberts, L. Goff, G. Pertea, D. Kim, D.R. Kelley, H. Pimentel, S.L. Salzberg, J.L. Rinn, and L. Pachter. 2012. Differential gene and transcript expression analysis of RNA-seq experiments with TopHat and Cufflinks. *Nat. Protoc.* 7:562–578. <https://doi.org/10.1038/nprot.2012.016>
- Tsagaratou, A., T. Äijö, C.W. Lio, X. Yue, Y. Huang, S.E. Jacobsen, H. Lähdesmäki, and A. Rao. 2014. Dissecting the dynamic changes of

- 5-hydroxymethylcytosine in T-cell development and differentiation. *Proc. Natl. Acad. Sci. USA*. 111:E3306–E3315. <https://doi.org/10.1073/pnas.1412327111>
- Uhlen, M., C. Zhang, S. Lee, E. Sjöstedt, L. Fagerberg, G. Bidkhor, R. Benfeitas, M. Arif, Z. Liu, F. Edfors, et al. 2017. A pathology atlas of the human cancer transcriptome. *Science*. 357:eaan2507. <https://doi.org/10.1126/science.aan2507>
- Vanharanta, S., W. Shu, F. Brenet, A.A. Hakimi, A. Heguy, A. Viale, V.E. Reuter, J.J. Hsieh, J.M. Scandura, and J. Massagué. 2013. Epigenetic expansion of VHL-HIF signal output drives multiorgan metastasis in renal cancer. *Nat. Med.* 19:50–56. <https://doi.org/10.1038/nm.3029>
- Varela, I., P. Tarpey, K. Raine, D. Huang, C.K. Ong, P. Stephens, H. Davies, D. Jones, M.L. Lin, J. Teague, et al. 2011. Exome sequencing identifies frequent mutation of the SWI/SNF complex gene PBRM1 in renal carcinoma. *Nature*. 469:539–542. <https://doi.org/10.1038/nature09639>
- Watanabe, Y., M. Toyota, Y. Kondo, H. Suzuki, T. Imai, M. Ohe-Toyota, R. Maruyama, M. Nojima, Y. Sasaki, Y. Sekido, et al. 2007. PRDM5 identified as a target of epigenetic silencing in colorectal and gastric cancer. *Clin. Cancer Res.* 13:4786–4794. <https://doi.org/10.1158/1078-0432.CCR-07-0305>
- Zhou, B., J. Wang, S.Y. Lee, J. Xiong, N. Bhanu, Q. Guo, P. Ma, Y. Sun, R.C. Rao, B.A. Garcia, et al. 2016. PRDM16 Suppresses MLL1r Leukemia via Intrinsic Histone Methyltransferase Activity. *Mol. Cell*. 62:222–236. <https://doi.org/10.1016/j.molcel.2016.03.010>
- Zhou, H., Y.H. Yang, and J.R. Basile. 2017. Characterization of the Effects of Semaphorin 4D Signaling on Angiogenesis. *Methods Mol. Biol.* 1493:429–441. [https://doi.org/10.1007/978-1-4939-6448-2\\_31](https://doi.org/10.1007/978-1-4939-6448-2_31)

**Supplemental material**

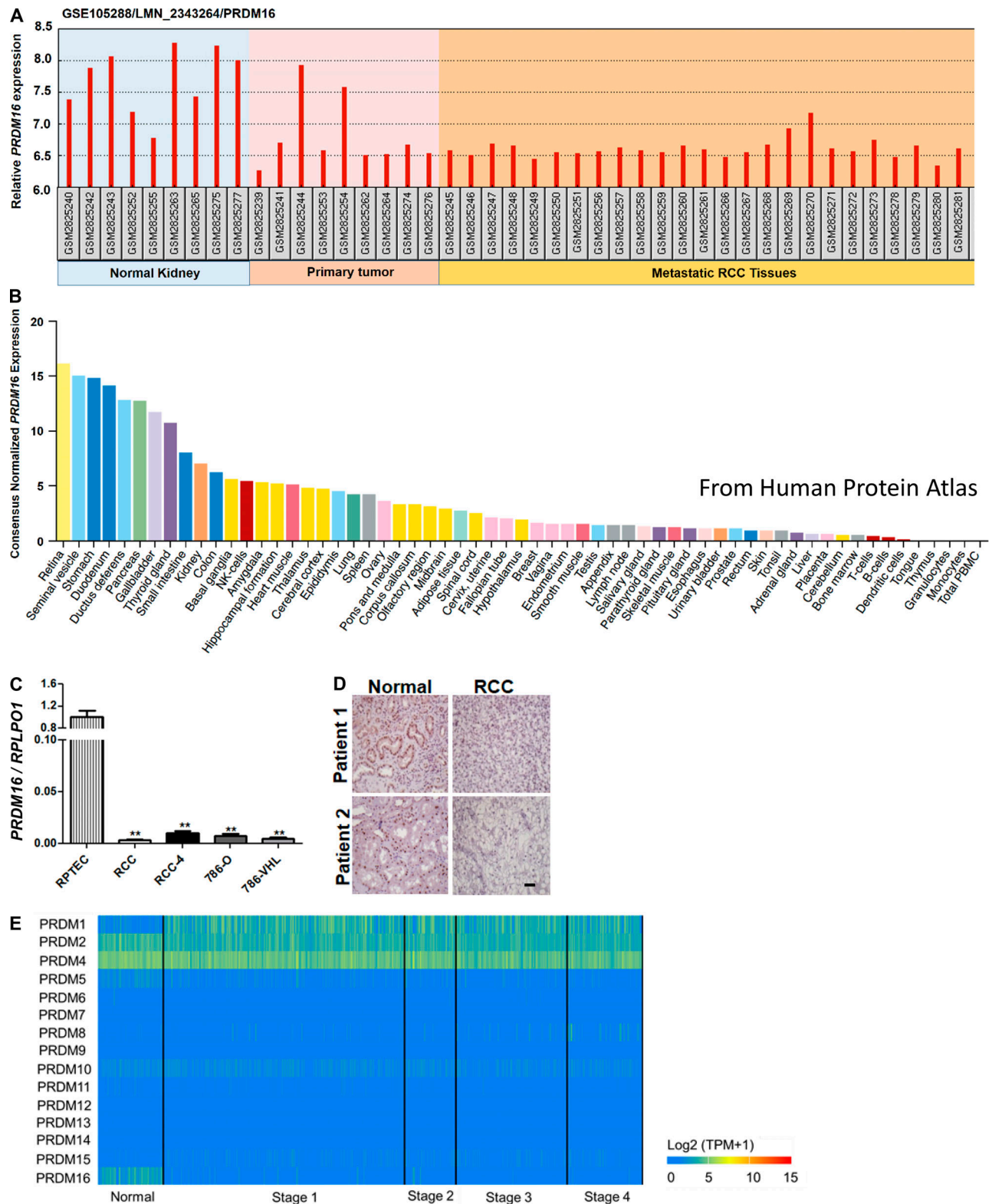


Figure S1. **PRDM16 expression in RCC.** (A) Relative PRDM16 expression in normal kidney ( $n = 9$ ), primary RCC ( $n = 9$ ), and metastatic RCC tissues ( $n = 26$ ) using the NCBI GEO2R analysis tool. Data are log<sub>2</sub> transformed. (B) Consensus tissue expression of PRDM16 from three transcriptomic datasets (Human Protein Atlas RNaseq data, GTEx, and CAGE data from the FANTOM5 project; <https://www.proteinatlas.org/ENSG00000142611-PRDM16/tissue>). (C) qPCR analysis of PRDM16 transcripts ( $n = 3$ ) from different RCC cell lines and from untransformed kidney cell line (RPTEC). RPLP01 was used as the reference gene. Data are relative with RPTEC expression normalized to 1. Data are mean  $\pm$  SD; Student's  $t$  test, \*\*,  $P < 0.005$ . (D) PRDM16 immunohistochemistry demonstrating nuclear staining in normal kidney with absence of staining in tumor tissues in matched normal/tumor patient samples ( $\times 400$  magnification; scale bar in black, 20  $\mu$ m). (E) Expression of PRDM family proteins in TCGA KIRC datasets using UALCAN web browser. C is a representative of two independent experiments.

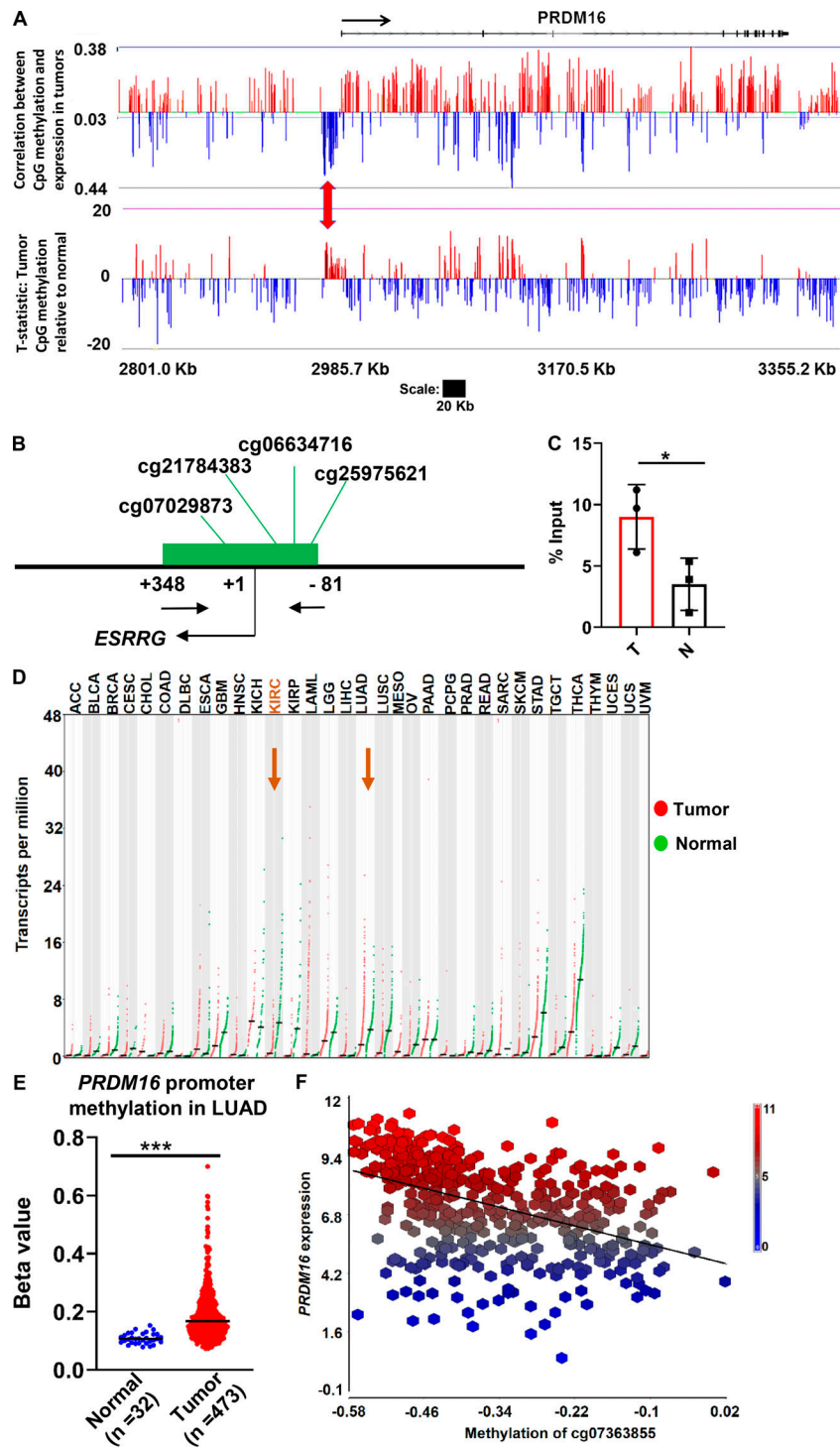


Figure S2. **PRDM16 promoter methylation.** (A) Top: Correlation analysis between individual CpG site methylation level and PRDM16 gene expression in tumors from the TCGA dataset. Blue and red color denote negative and positive correlation, respectively. Bottom: T-statistic comparing CpG site methylation in the region of PRDM16 locus in tumor relative to normal kidney. A positive T-statistic (shown as red peaks) indicates the tumor was more methylated than the normal, whereas a negative T-statistic (shown as blue peaks) indicates the tumor was less methylated than the normal. The higher the absolute value of the T-statistic, the greater the significance. Genomic coordinates (chromosome 1) from the UCSC genome browser are shown at the bottom. (B and C) Schematic representation of the ESRRG promoter region previously identified as hypermethylated in RCC. Black arrows demote primer pair located within CpG island (green bar) used to analyze 5mC enrichment by 5mC-ChIP in tumor (T)-normal (N) pairs ( $n = 3$ ). Data are mean  $\pm$  SD; Student's  $t$  test, \*,  $P < 0.05$ . (D) Analysis of PRDM16 gene expression via GEPIA web portal across different normal-tumor samples in TCGA. KIRC and lungs adenocarcinoma (LUAD) datasets are highlighted by brown arrows. Black horizontal line represents the median. (E) Analysis of methylation in the PRDM16 promoter region via UALCAN web portal in LUAD in which PRDM16 expression is low. Black horizontal line represents the median. Student's  $t$  test, \*\*\*,  $P < 0.0001$ . (F) Plot of PRDM16 mRNA relative expression (y axis) as a function of methylation ( $\beta$ ) level (x axis) at CpG locus cg07363855, which demonstrates increased methylation in LUAD.  $\beta$  levels are all mean-centered.

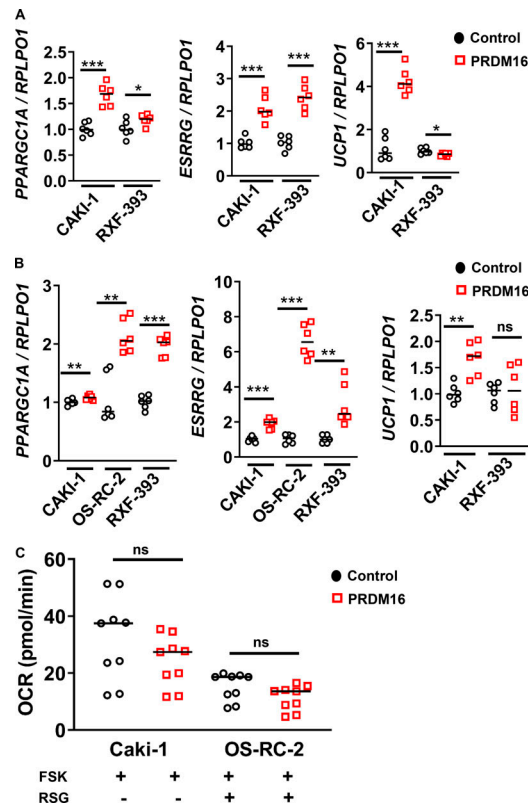


Figure S3. **Effect of PRDM16 on the expressions of mitochondrial metabolism-related transcription factors using forskolin and rosiglitazone in RCC cell lines.** **(A)** qPCR analysis of *PPARGC1A*, *ESRRG*, and *UCP1* transcripts in RCC cell lines (Caki-1 and RXF-393;  $n = 6$ ) stably transduced with either control vector or PRDM16 and treated with  $10 \mu\text{M}$  forskolin for 4 h. **(B)** qPCR analysis of *PPARGC1A*, *ESRRG*, and *UCP1* transcripts in RCC cell lines (Caki-1, OS-RC-2, and RXF-393;  $n = 6$ ) stably transduced with either control or PRDM16 and treated with  $1 \mu\text{M}$  rosiglitazone and  $10 \mu\text{M}$  forskolin for 24 h. Data in A and B are normalized to control vector and are representative of two independent experiments. **(C)** OCR analysis of stably transduced plus or minus PRDM16 Caki-1 and OS-RC-2 cells treated either with forskolin ( $10 \mu\text{M}$ ) for 4 h or with forskolin ( $10 \mu\text{M}$ ) and rosiglitazone ( $1 \mu\text{M}$ ) for 24 h. Data are mean  $\pm$  SD. Student's *t* test, \*,  $P < 0.05$ , \*\*,  $P < 0.005$ , and \*\*\*,  $P < 0.0001$ ; ns, not significant.

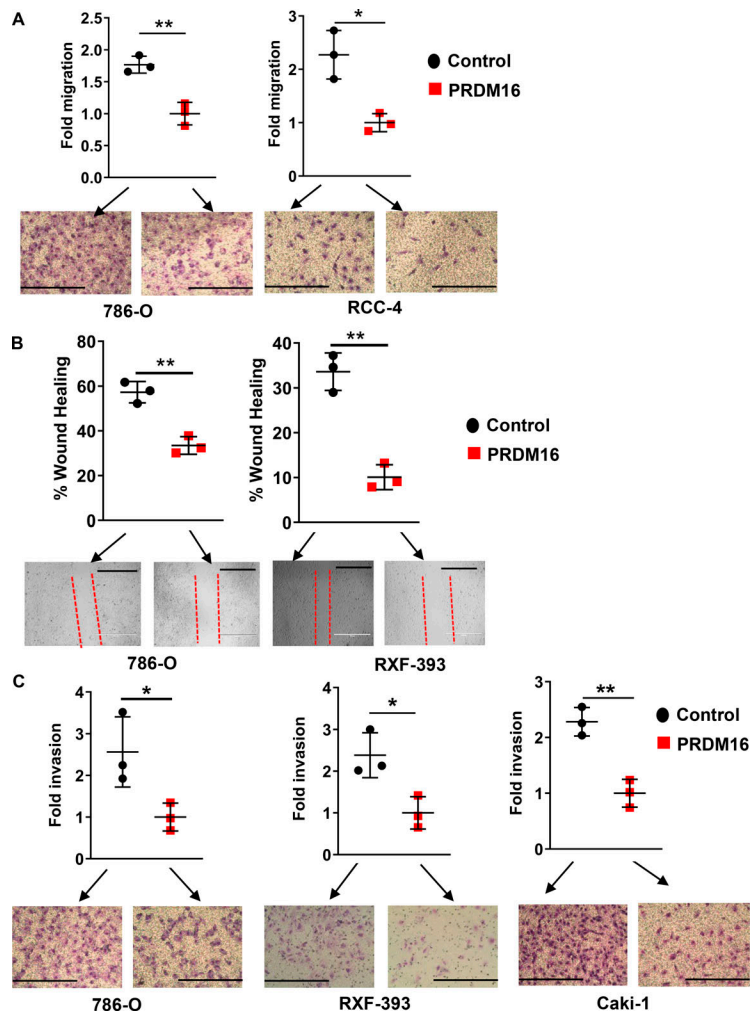


Figure S4. **Effect of PRDM16 on migratory, wound healing, and invasive properties of RCC cells.** (A–C) Migration, wound healing, and invasion assays of RCC cells (786-O, RCC4, RXF-393, and Caki-1) stably transduced ( $n = 3$ ) with either control vector or PRDM16. Migration and invasion assays were performed over 16 h. Wound healing assay was performed over 9 h. Data are representative of at least three independent experiments. Scale bars in black, 1,000  $\mu\text{m}$ . Data are mean  $\pm$  SD. Student's  $t$  test, \*,  $P < 0.05$  and \*\*,  $P < 0.005$ .

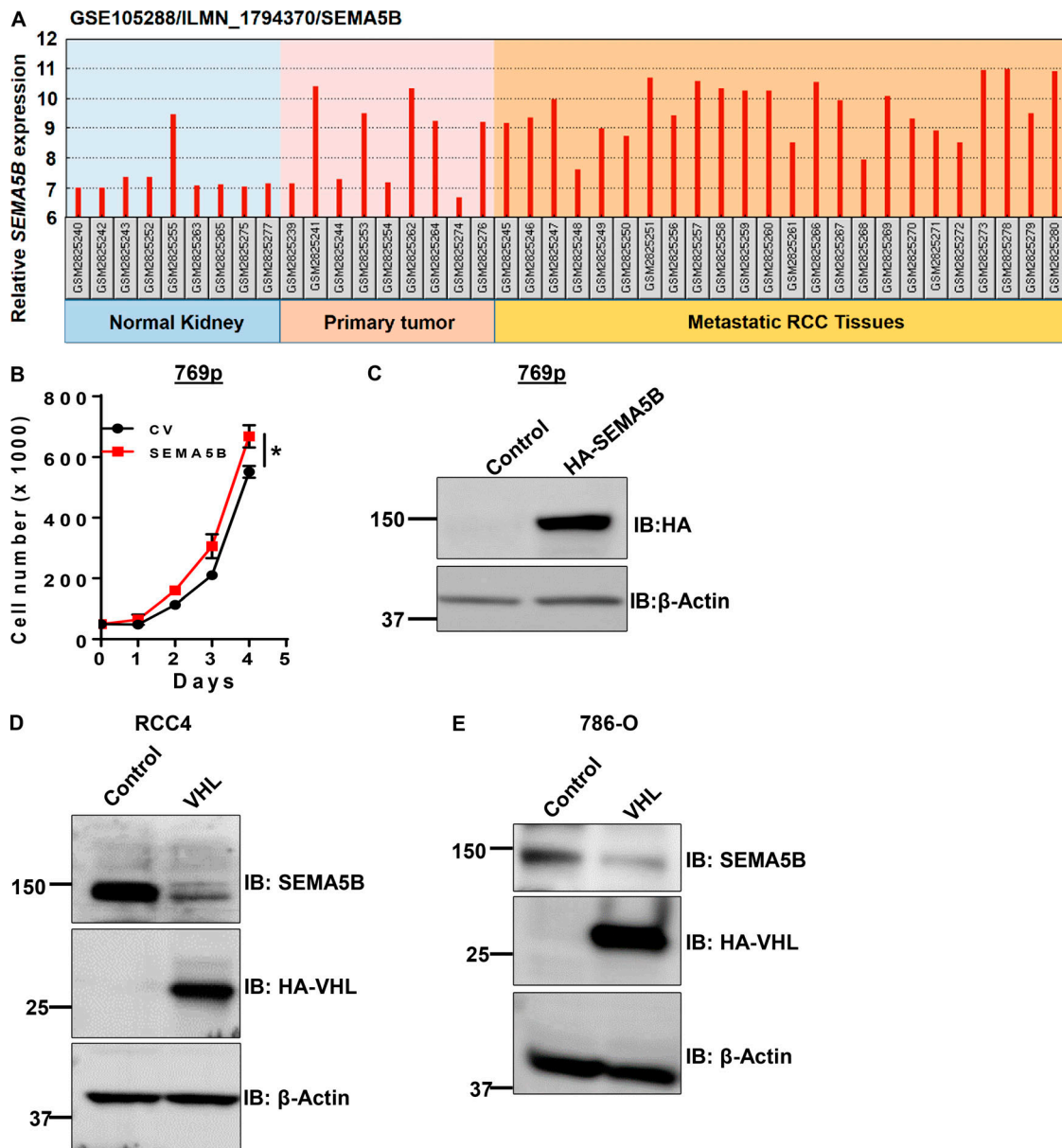


Figure S5. **SEMA5B effect on proliferation and regulation by VHL.** (A) Relative SEMA5B expression in normal kidney ( $n = 9$ ), primary RCC ( $n = 9$ ), and metastatic RCC tissues ( $n = 26$ ) using the NCBI GEO2R analysis tool. (B and C) 769p cells stably transduced ( $n = 3$ ) with either control vector or HA-SEMA5B and assayed for proliferation and for (C) SEMA5B (HA-tagged) protein levels. Data are mean  $\pm$  SD. (D and E) RCC4 (D) and 786-O (E) were stably transduced with either control vector or HA-VHL. Cell lysates were immunoblotted for endogenous SEMA5B. Data in B–E are representative of two independent experiments. Student's  $t$  test, \*,  $P < 0.05$ .

Tables S1–S3 are provided online as separate Excel files. Table S1 shows differential expression of the top 250 genes from RCC tissues and normal kidney. Table S2 shows RNaseq analysis of 786-O cells expressing PRDM16 or CV and gene ontology analysis of 786-O cells expressing PRDM16 or CV. Table S3 shows LC-MS analysis of PRDM16 (Flag)-interacting proteins.